AD-A194 247 EFFECTS OF TECTONIC RELEASE ON BROADBAND REGIONAL DISTANCE BODYWAVES(U) ARIZONA UNIV TUCSON T C WALLACE ET AL. 01 NOV 87 AFGL-TR-87-0239 1/1

UNCLASSIFIED F19628-85-K-0014 F/G 17/10 NL

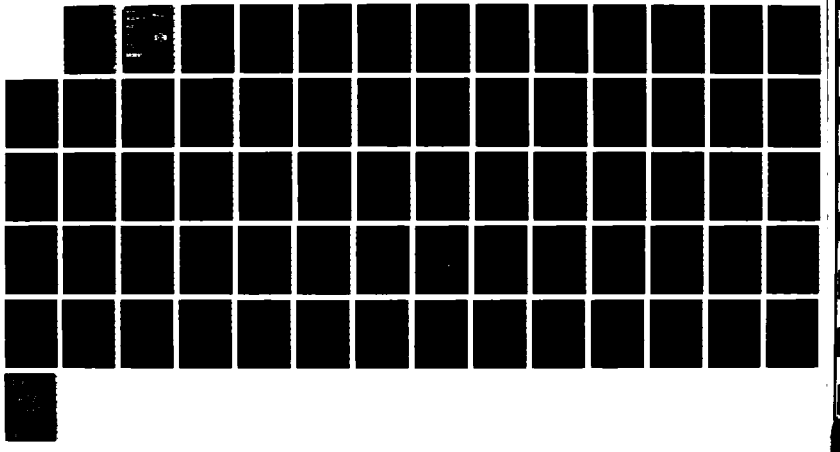

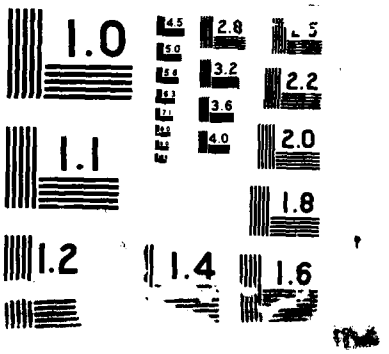
1.0
1.1
1.2
1.4
1.6
1.8
2.0
2.2
2.8
3.2
3.6
4.0
4.5
5.0

(4)

[illegible]-TR-87-0230

Effects of Tectonic Release on Broadband Regional Distance Bodywaves

Terry C. Wallace
William E. Holt
Kim Junkyoung

University of Arizona
Tucson, AZ 85721

1 November 1987

Final Report
January 1985-January 1987

APPROVED FOR PUBLIC RELEASE; DISTRIBUTION UNLIMITED

AIR FORCE GEOPHYSICS LABORATORY
AIR FORCE SYSTEMS COMMAND
UNITED STATES AIR FORCE
HANSCOM AIR FORCE BASE, MASSACHUSETTS 01731

Unclassified

SECURITY CLASSIFICATION OF THIS PAGE

A194247

REPORT DOCUMENTATION PAGE

1a. REPORT SECURITY CLASSIFICATION Unclassified	1b. RESTRICTIVE MARKINGS
2a. SECURITY CLASSIFICATION AUTHORITY	3. DISTRIBUTION/AVAILABILITY OF REPORT Approved for public release; distribution unlimited
2b. DECLASSIFICATION/DOWNGRADING SCHEDULE	
4. PERFORMING ORGANIZATION REPORT NUMBER(S)	5. MONITORING ORGANIZATION REPORT NUMBER(S) AFGL-TR87-0239
6a. NAME OF PERFORMING ORGANIZATION University of Arizona 6b. OFFICE SYMBOL (If applicable)	7a. NAME OF MONITORING ORGANIZATION Air Force Geophysics Laboratory.
6c. ADDRESS (City, State and ZIP Code) Tucson, AZ 85721	7b. ADDRESS (City, State and ZIP Code) Hanscom AFB Massachusetts 01731
8a. NAME OF FUNDING/SPONSORING ORGANIZATION DARPA 8b. OFFICE SYMBOL (If applicable) STO/GSD	9. PROCUREMENT INSTRUMENT IDENTIFICATION NUMBER F19628-85-K-0014
8c. ADDRESS (City, State and ZIP Code) 1400 Wilson Boulevard Arlington, VA 22209-2308	10. SOURCE OF FUNDING NOS. PROGRAM ELEMENT NO.: 62101F PROJECT NO.: 5A10 TASK NO.: DA WORK UNIT NO.: AG
11. TITLE (Include Security Classification) Effects of Tectonic Release on Broadband Regional Distance Bodywaves	
12. PERSONAL AUTHOR(S) Terry C. Wallace, William E. Holt, Kim Junkyoung	
13a. TYPE OF REPORT Final Report 13b. TIME COVERED FROM 1/1985 TO 1/1987	14. DATE OF REPORT (Yr., Mo., Day) 11/1/87 15. PAGE COUNT 68
16. SUPPLEMENTARY NOTATION	

17. COSATI CODES			18. SUBJECT TERMS (Continue on reverse if necessary and identify by block number)
FIELD	GROUP	SUB. GR.	Tectonic release, underground nuclear explosions, seismic waves

19. ABSTRACT (Continue on reverse if necessary and identify by block number)

The effects of tectonic release on regional distance and near-field seismograms from nuclear explosions have been investigated by modeling with synthetic seismograms and moment tensor inversion. Although the distortion of explosion long-period waves is documented at upper mantle distances, the signature is much more subtle at regional and near-field distances. We document the robustness of the observation of sP in the explosions waveforms of events which have large F factors. Although "slapdown" has not been added to the synthetics, the strong azimuthal variation can be explained by the simple addition of a double couple (tectonic release). We also calibrate the size of tectonic release for 18 Pahute Mesa events by comparing their SH waves with those of two western United States earthquakes.

(over)

20. DISTRIBUTION/AVAILABILITY OF ABSTRACT UNCLASSIFIED/UNLIMITED ☐ SAME AS RPT. ☐ DTIC USERS ☐	21. ABSTRACT SECURITY CLASSIFICATION Unclassified
22a. NAME OF RESPONSIBLE INDIVIDUAL James Lewkowicz	22b. TELEPHONE NUMBER (Include Area Code) (617) 377-3028 22c. OFFICE SYMBOL AFGL/LWH

DD FORM 1473, 83 APR EDITION OF 1 JAN 73 IS OBSOLETE.

SECURITY CLASSIFICATION OF THIS PAGE

19. ABSTRACT (continued)

In general, the signature of tectonic release appears to be strongly frequency-dependent. We have performed a moment tensor inversion at three Pahute Mesa events (CHESIRE, FARM and POOL) in different frequency bands in an attempt to isolate the "dispersion" of the deviatoric component of the moment tensor. Although the apparent size of tectonic release source decreases, the orientation appears to be constant. The moments of the tectonic release at regional distance also are inconsistent with near-field estimates. We have developed a model for near-field tectonic release, which requires a distributed source (shear dislocation takes place at the elastic radius). Using BOXCAR and HALFBEAK waveforms, we performed a constrained moment tensor inversion to obtain the tectonic release orientation. This near-field orientation is in excellent agreement with the far-field results.

Many earthquakes have sparse waveform data sets, requiring any inversion procedure for source parameters to account for data from widely different distances. Here we present a procedure for the joint inversion of regional and teleseismic long-period waveforms for source parameter estimates. With three test cases we demonstrate that the inclusion of regional distance seismograms to a data set of teleseismic observations stabilizes the inversion process and adds valuable constraints to the source parameter estimates, particularly when the teleseismic Green's functions are inadequate. The added stability and constraints from regional waveforms can be attributed to the robust nature of regional distance Green's functions, as well as the added coverage of the focal sphere that regional waveforms provide. Singular value decomposition is a useful inversion method that is well suited for this study because it allows the determination of the influence that individual observations are having on the model parameter estimates.

TABLE OF CONTENTS

		Page
I.	INTRODUCTION	1
II.	EVIDENCE FOR A SHORT-PERIOD TECTONIC RELEASE SIGNATURE	4
III.	FREQUENCY DEPENDENCE OF TECTONIC RELEASE AT REGIONAL DISTANCES	17
IV.	NEAR-FIELD TECTONIC RELEASE	28
V.	JOINT INVERSION OF REGIONAL AND TELESEISMIC WAVEFORMS	34
	REFERENCES	49

I. INTRODUCTION

One of the main consequences of decreasing the yield limit in a threshold test ban is the increased reliance on regional distance seismograms for monitoring purposes. Most schemes for determining the yield at regional distances are based on measuring the amplitude of phases such as Pg and Lg. It is extremely important to a TTBT to understand the nature of propagation at these phases in different regions, as well as possible sources of bias such as tectonic release. Here we report on our continuing research on tectonic release.

It is presently thought that surface waves provide the best data for determining the orientation of the equivalent double couple representation of tectonic release. The main reason for this is that until recently there has been very little documentation of the influence of tectonic release on P waves. The most widely accepted explanation for the lack of an obvious tectonic release signature on short-period P waves is that the tectonic release is a low stress drop phenomena (Bache, 1976). In the case of NTS, the low stress drop will conspire with the strike-slip radiation pattern (which does not radiate P waves efficiently to teleseismic distances) predicted for the tectonic release to make the short-period signature very difficult to observe in the far-field body waves. The strongest evidence that tectonic release can radiate high frequency energy is presented in Wallace et al. (1983, 1985), where it is shown that at regional distances the long-period P waves have complexity which correlates with the size of the SV amplitude--suggesting a shear-dislocation source. Further, the SH waves can be modeled with a strike-slip orientation. Recently this interpretation of the P wave complexity has been reinterpreted as "slapdown" (Douglas et al., 1986). In Section II we investigate this possibility, and once again conclude that the simplest explanation is tectonic release. Further,

the long-period tectonic release orientation (surface waves) correlates very well with the azimuthal variability of the short-period P waves.

There is an apparent frequency dependence of the tectonic release signature at regional distances. At periods of 5-15 seconds, Wallace et al. (1983) show that the P_{nl} waveforms from Pahute Mesa explosions are sometimes strongly distorted by tectonic release, which amounts to superimposing the explosion and a strike-slip earthquake source. On the other hand, Alexander (1980), Pomeroy et al. (1982) and Gupta and Blandford (1983) present results which indicate that tectonic release has little effect on 3-Hz Lg amplitudes. A similar problem is rectifying the far-field representation of the tectonic release with the observations of the tangential component of strong ground motion. The observed near-field SH waves from Pahute Mesa events are much more complicated and significantly smaller than expected. Usually the near-field SH waves are interpreted in terms of scattered energy. In Section III we discuss the frequency dependence of the tectonic release signature at regional distances. The only plausible explanation for the apparent dispersion is a shift in the corner frequency. This is consistent with the results discussed in Section IV, in which we have developed a "distributed" model for tectonic release.

Any routine inversion procedure developed to recover tectonic release source parameters will require the analysis of sparse data sets, requiring the use of waveforms from widely different distances. In Section V we present a procedure for the joint inversion of regional and teleseismic long-period waveforms for source parameter estimates. With three test cases we demonstrate that the inclusion of regional distance seismograms to a data set of teleseismic observations stabilizes the inversion process and adds valuable constraints to the source parameter estimates, particularly when the teleseismic Green's functions are inadequate. The added stability and constraints from regional waveforms can be attributed to the robust nature of regional distance Green's functions, as well as the added coverage of the focal sphere that regional waveforms provide. Singular value decomposition is a useful inversion

method that is well suited for this study because it allows the determination of the influence that individual observations are having on the model parameter estimates.

II. EVIDENCE FOR A SHORT-PERIOD TECTONIC RELEASE SIGNATURE

In two earlier papers (Wallace et al., 1983, 1985), we discussed the evidence for tectonic release from underground nuclear explosions on Pahute Mesa at the Nevada Test Site (NTS) as observed in long-period body waves. It has been shown for some time that the nonisotropic component of the surface waves from most of these events could be explained by an equivalent double-couple source, namely strike-slip motion on north-striking faults. In an attempt to get better resolution on the mechanism of the tectonic release, we modeled the SH wave forms using the constraints imposed by reversals in the SV polarity and distortions in the long-period P waves. We found that the orientation inferred from the body waves closely matched those determined from the surface waves. Further, we were able to determine the seismic moments for the tectonic release by comparison with several shallow, strike-slip earthquakes. Although the SH waveforms provide the most direct measure of the tectonic release, the tectonic release mechanism adequately explains a wide range of long-period body wave observations. In particular, we identified a distortion in the upper mantle long-period P waves which we attribute to the phase SP from the tectonic release. The amplitude of this phase correlates very well with the moment of the tectonic release; it can be modeled by adding a strike-slip synthetic to the waveform of a low tectonic release event (see Figure II-1); and finally it shows a change in polarity (Figure II-2) as expected by the strike-slip radiation pattern. The identification of the sP phase provided the highest frequency signature of tectonic release (0.33 Hz) yet known and suggested that short-period P waves could also be affected by tectonic release. With this in mind, Lay et al. (1984) studied the first cycle (ab) amplitude of the teleseismic short-period P waves from the Pahute Mesa events and found a

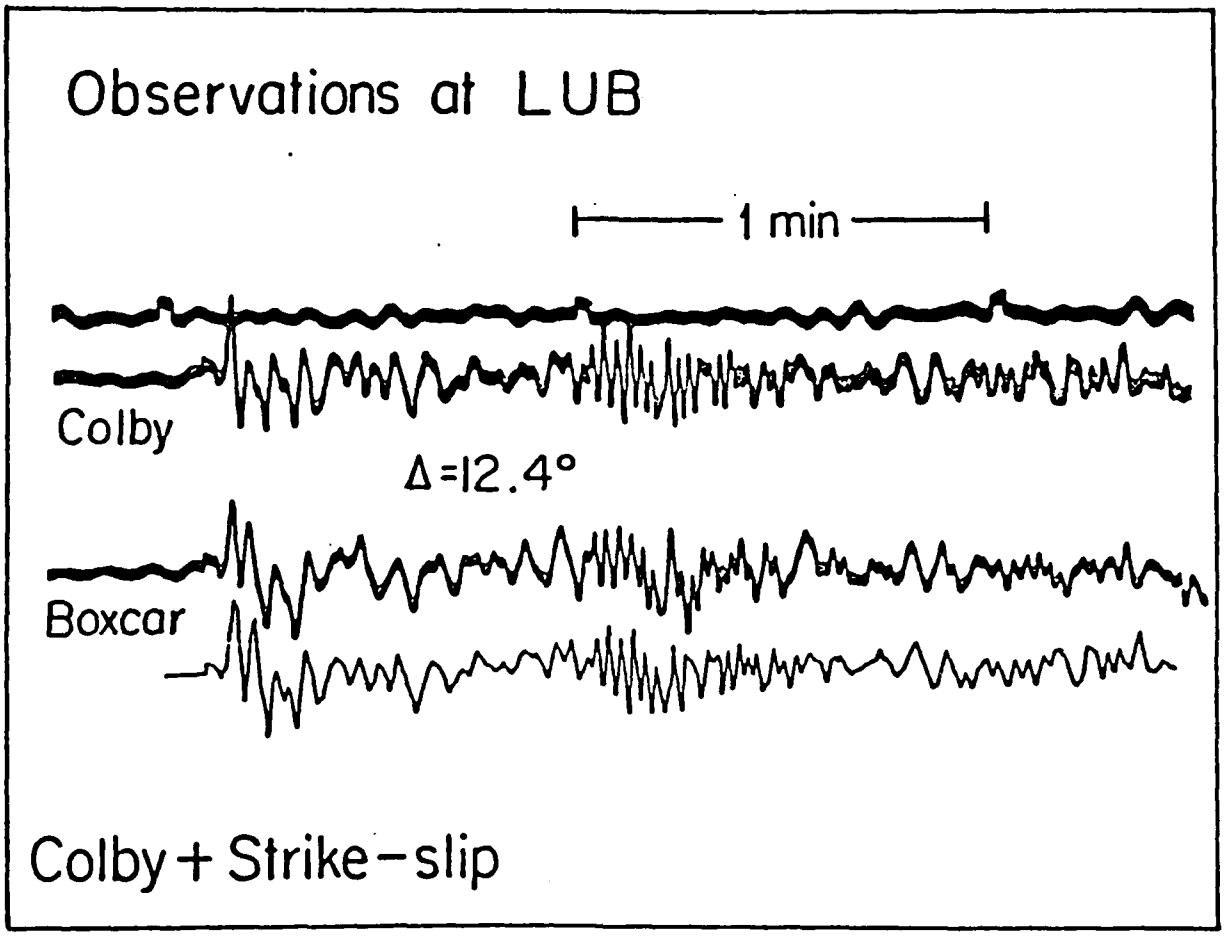

Figure II-1: A comparison of the P and PL waves for BOXCAR and COLBY at LUB. Shown below is the COLBY waveform summed with a synthetic seismogram to simulate the tectonic release. The double couple has a pure strike-slip orientation. The time function is a triangle with a 0.6 second duration. The seismic moment for the double couple required to obtain the fit is 5×10^{24} dyne-cm.

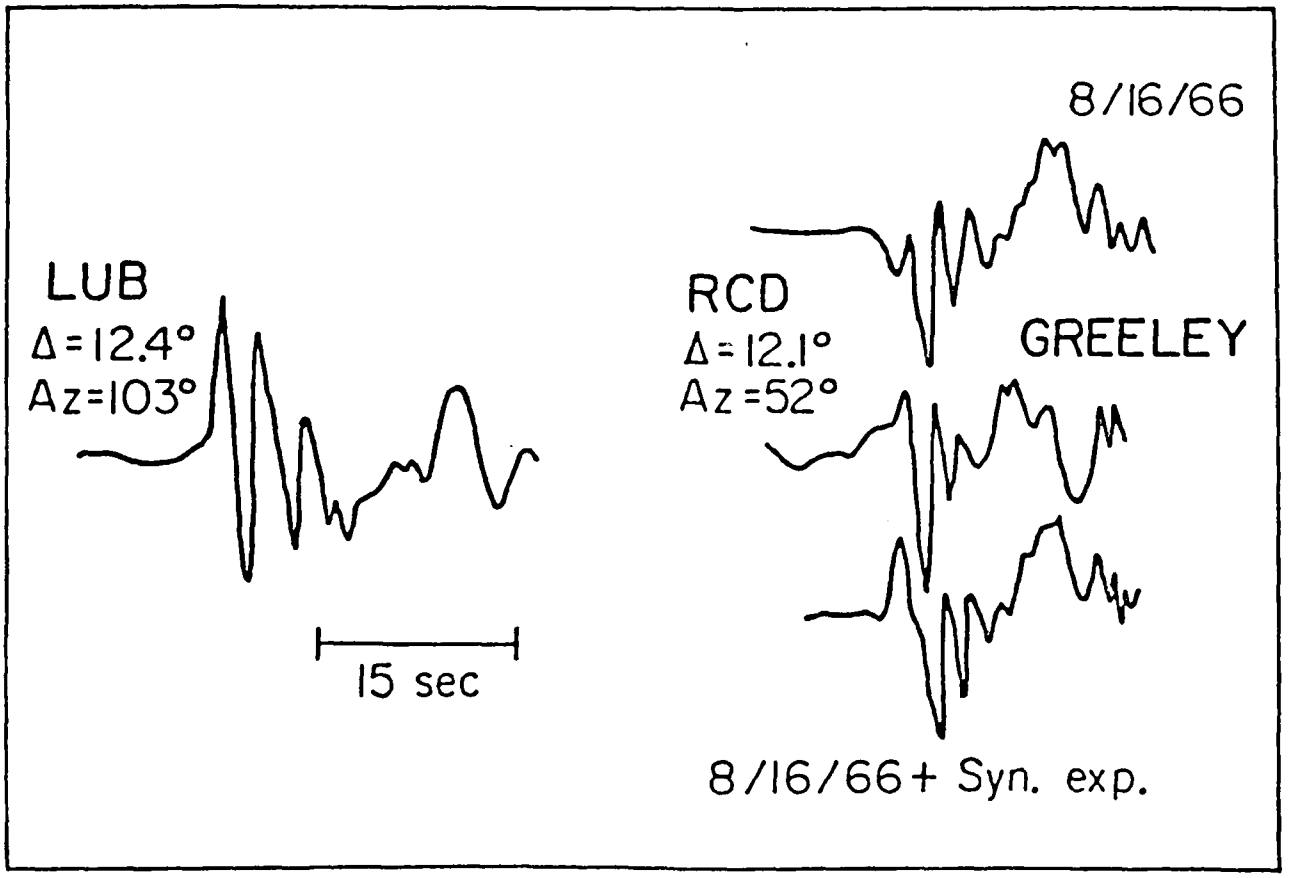

Figure II-2: A comparison of the GREELEY waveforms at LUB and RCD. Also shown is the waveform of the 8-16-66 earthquake. This earthquake was used to simulate the GREELEY record by summing with a synthetic explosion waveform.

systematic azimuthal variation which is consistent with a distortion which could be caused by the tectonic release.

There is some controversy over our interpretation of the long-period body wave tectonic release signature. Douglas et al. (1986) suggest that we have misinterpreted the complexity in the P waves, and actually the distortion is caused by slapdown, and that there is no evidence to support that tectonic release is influencing the first P wave arrivals from explosions at NTS. The principal data Douglas cites are the broadband recordings at EKA of the large Pahute Mesa events (Figure II-3). If our interpretation of tectonic release is correct, Douglas contends that the deflection he has marked Ao should have a negative polarity, which it does not. It is important to note here that these backswings in the P waves are interference patterns between the explosion P, pP, and any contribution of slapdown with that of the sP phase is from the tectonic release. Such interference patterns are very sensitive to the relative timing of the different episodes. A small shift in the location of the tectonic release relative to the explosion can produce a "misleading" polarity. A direct comparison between II-3 and Figure II-4 shows that, in fact, the backswing in question is greatly reduced relative to direct P for the high tectonic release events such as MUENSTER and BENHAM at 5 EKA, which is consistent with the tectonic release interpretation. It also must be remembered that SHA (the station Wallace et al. used for comparison) is 24° from NTS, while EKA is approximately 70° away. This change in distance corresponds to a change in the surface reflection coefficient of sP from -0.55 to -0.36; or a reduction by one-third at EKA as compared to SHA.

We want to reiterate that the reason we favor the interpretation that tectonic release can have a signature on long-period P waves is its consistency with a large data set. The amplitude of the sP phase is consistent with that predicted on the basis of the SH waves. The SV phase from BENHAM and GREELEY shows a phase reversal which is consistent with the orientation determined for the tectonic release double couple. The SV reversal is

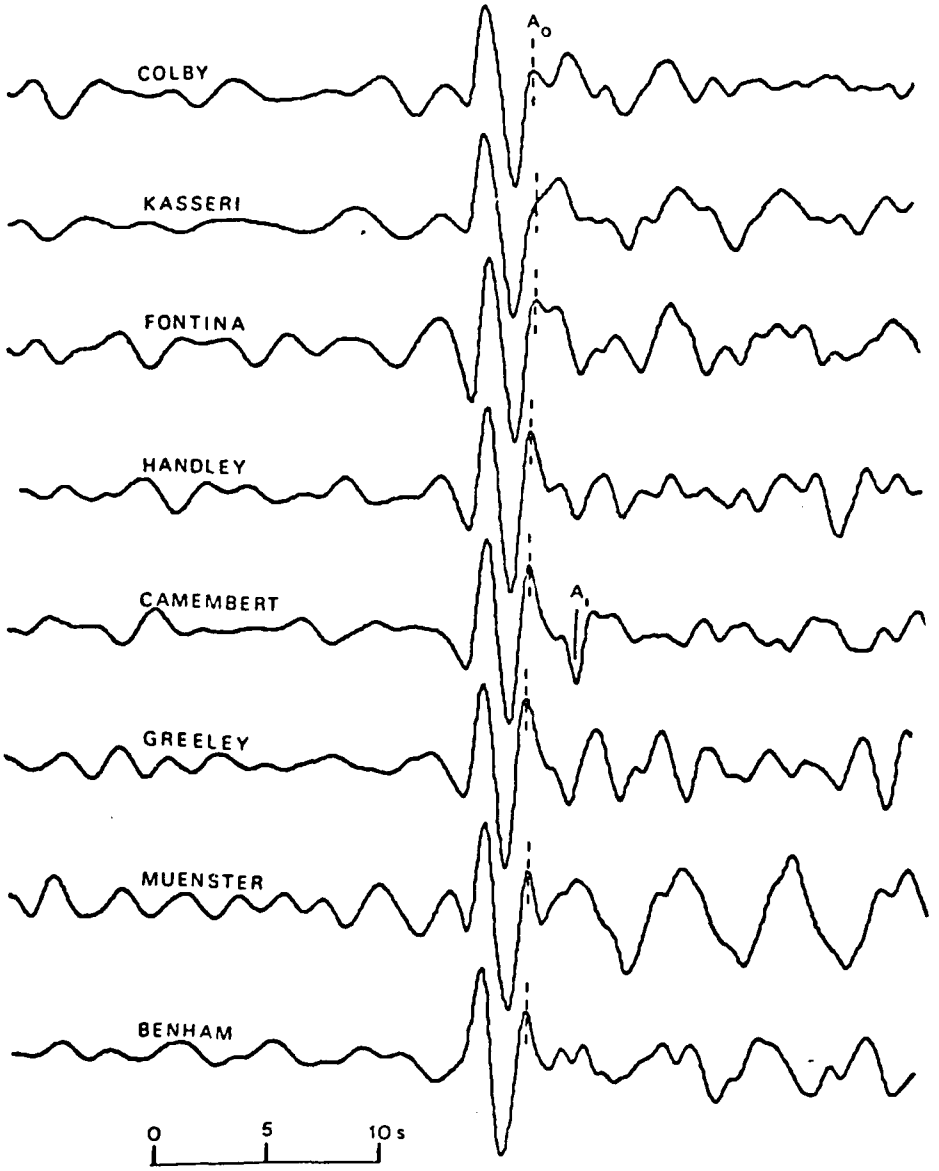

Figure II-3: Broadband P wave seismograms from eight Pahute Mesa explosions recorded at ESK (from Douglas et al., 1986). Douglas identifies A_o as slapdown, and A_1 as an aftershock.

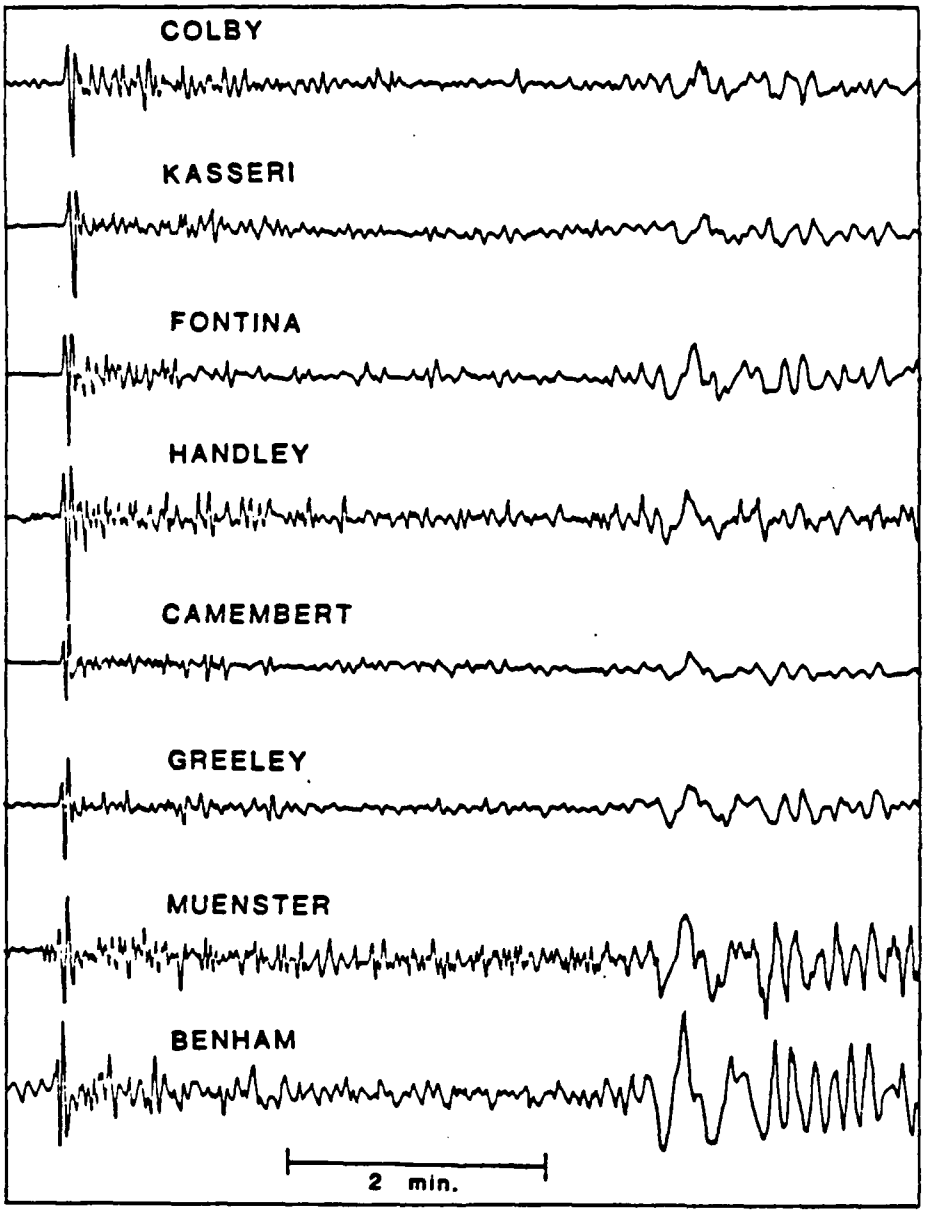

Figure II-4: The vertical component records for 8 large Pahute Mesa explosions at the WWSSN station SHA. These are long-period seismograms which are arranged according to the importance of the second upswing in the P wave. About 4½ minutes after the P arrival is the SV wave.

accompanied by a reversal in polarity of the phase we have identified as sP. The long-period regional distance body waves (P_{nl}) also show a distortion which is consistent with the interference from strike-slip tectonic release. In the case of the P_{nl} waveforms, the signature is over a 45-sec window rather than a single arrival (sP). Although we have not modeled slapdown, and as Douglas et al., point out, it can have an effect on the long-period P waves, we believe it cannot account for all the observations listed above. In particular, slapdown cannot produce the four-lobed SH radiation pattern, nor the polarity reversal of sP. Further, one of the most remarkable facts about the tectonic release from NTS is its consistency in orientation. With only two or three exceptions (HALFBREAK and PILEDRIVER), the tectonic release is predominantly strike-slip motion on north-trending planes. It is very difficult to appeal to a form of explosion source anisotropy or slapdown that will always produce an identical apparent double-couple radiation pattern.

The question of whether the tectonic release has a signature at the frequencies of short-period P waves is a separate matter. For the most part, the short-period waveforms are quite complicated, and no one has convincingly identified an equivalent of the long-period sP phase. Lay et al. (1984) simply plotted the corrected ab amplitude of 25 Pahute Mesa explosions versus azimuth and noted that they appeared to have a sin (2ϕ) variation. Lay et al. found that the best fit of a sin (ϕ) curve to the amplitudes was consistent with the pattern that would be expected from the azimuthal radiation pattern for a vertical strike-slip fault with the orientation given by the analysis of the long-period SH waveforms. The significance of the sin (ϕ) fit was evaluated with an f-test. Nearly all the Pahute Mesa explosions pass the test at the 99th per cent level, but most importantly, the events with the largest long-period tectonic release show the clearest sin (2ϕ) pattern. There are alternative explanations for the amplitude behavior, such as upper mantle structure beneath Pahute Mesa (Lynne and Lay, 1984) but again the consistency with all the other tectonic release data suggest that the ab amplitude "could be" modulated by a strike-slip radiation pattern.

Lay et al. also cite differences in waveform between stations near the node and those in the lobe as evidence of tectonic release. Douglas et al. suggest that the change in waveform is due to lateral variations in attenuation. In particular, they map the loop station (UME) into the node station (OGD) by increasing t^* by a factor of 2 (see Figure 4 in Douglas et al.). One way to test this path bias hypothesis is to compare UME and OGD for FAULTLESS, which was detonated 100 km north of Pahute Mesa; the waveforms for the two stations are nearly identical (see Lay et al., Figure 11). Further, we can test the stability of the sin (2ϕ) pattern from the Pahute Mesa events by comparing them to FAULTLESS. Figure 7 in Lay et al. shows that amplitude pattern from FAULTLESS is significantly different from that of GREELEY; in fact, they are nearly reversed. If one wants to appeal to attenuation to produce the sin (2ϕ) pattern, then it must also account for the FAULTLESS pattern. It seems unlikely that slight travel path differences between FAULTLESS and GREELEY to teleseismic distance stations would produce the factor of 5 change in relative amplitude.

Recently, Given and Mellman (1985) have analyzed the surface waves from several of the Pahute events using sophisticated phase velocity and attenuation correction developed for NTS by Stevens et al. (1982). Given and Mellman determined an orientation for the nonisotropic radiation which we have plotted against the strike of sin (2ϕ) pattern observed by Lay et al. (1984) for a set of eight events in Figure II-5. The strike of the double couple varies from 90° to 65° for the different events. Although there is some difference in the absolute value of the strikes as determined by the surface and body waves, their agreement is good. More remarkable is that fact that as the strike varies, the short periods track the long periods very well. It should be noted that this correlation breaks down for events outside or near the edge of Silent Valley Caldera. Again, the point of the figure is that the short-period P waves amplitudes correlate with the long-period tectonic release. Neither structure nor attenuation can be ruled out as causing the short-period pattern, but there is no reason that the short-

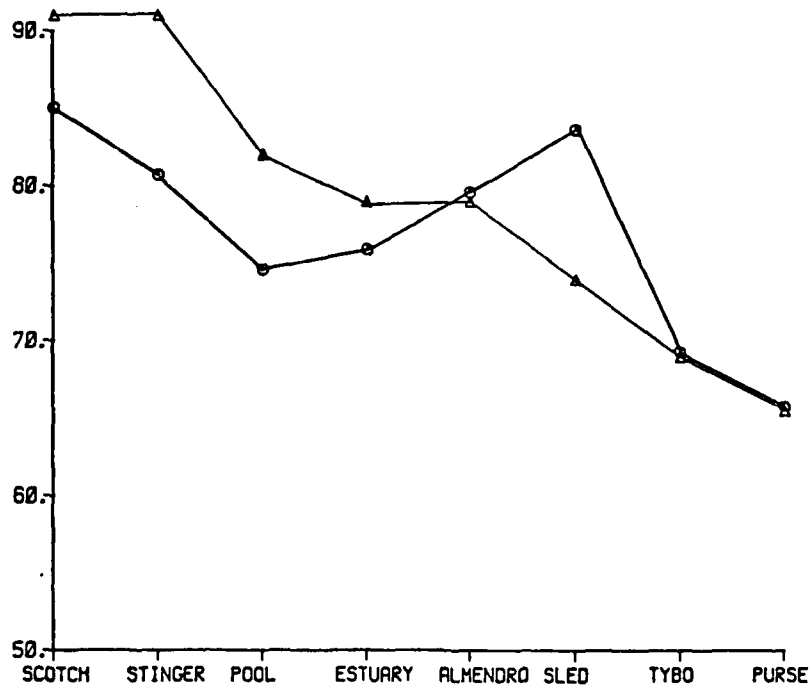

Figure II-5: Strike (in degrees) of the tectonic release double couple as determined from long-period surface waves (triangular symbols) compared with the strike of the sin (2ϕ) azimuthal variation observed in the ab amplitude of the short-period P waves. All of the events are within silent Canyon Caldera.

period P waves should correlate with long-period Love and Rayleigh waves unless tectonic release is causing the modulation.

One difficulty with our 1985 paper is the large moments we determined for the tectonic release. These values were determined on the basis of comparison of SH waves from two earthquakes: (1) 16 August 1966, near the Nevada-Utah border, and (2) 15 March 1979, in Homestead Valley in south central California. The moment values were very consistent from station to station when compared to either earthquake. Unfortunately, the average values for a given explosion varied by a factor of 2 depending on the reference earthquake. The 16 August 1966 earthquake gave moments which were twice those determined using the 15 March 1979 event. Since we did not know which estimate was more reliable, we averaged the values to produce Table I in the 1985 paper. Since that publication, several investigators have shown that there is a strong velocity variation across the Rocky Mountain front (Grand and Helmberger, 1984). Since the 16 August 1966 earthquake is along the front, it is probably inappropriate to use it as a calibration for NTS. Helmberger et al. (1985) have developed a lateral varying model for the North American continent. We used this model to construct synthetic seismograms for a strike-slip orientation and compare them to GREELEY in Figure II-6. As can be seen, the waveform fit is quite good; the average moment we obtain is 1.9 X 10^{24} dyne-cm, which is in very close agreement with the value we determine for GREELEY by the comparison with the 15 March 1979 earthquake. On the basis of this, we have revised the moments for tectonic release for 21 Pahute Mesa events. The new values are given in Table II-1.

Since our revised moments are smaller, the potential for tectonic release to influence the short-period P waves is also reduced. Although we are confident that tectonic release can have an identifiable signature in long-period P waves (2 to 5 sec), it has not conclusively been shown that it influences short-period P waves. The only way to address the question of

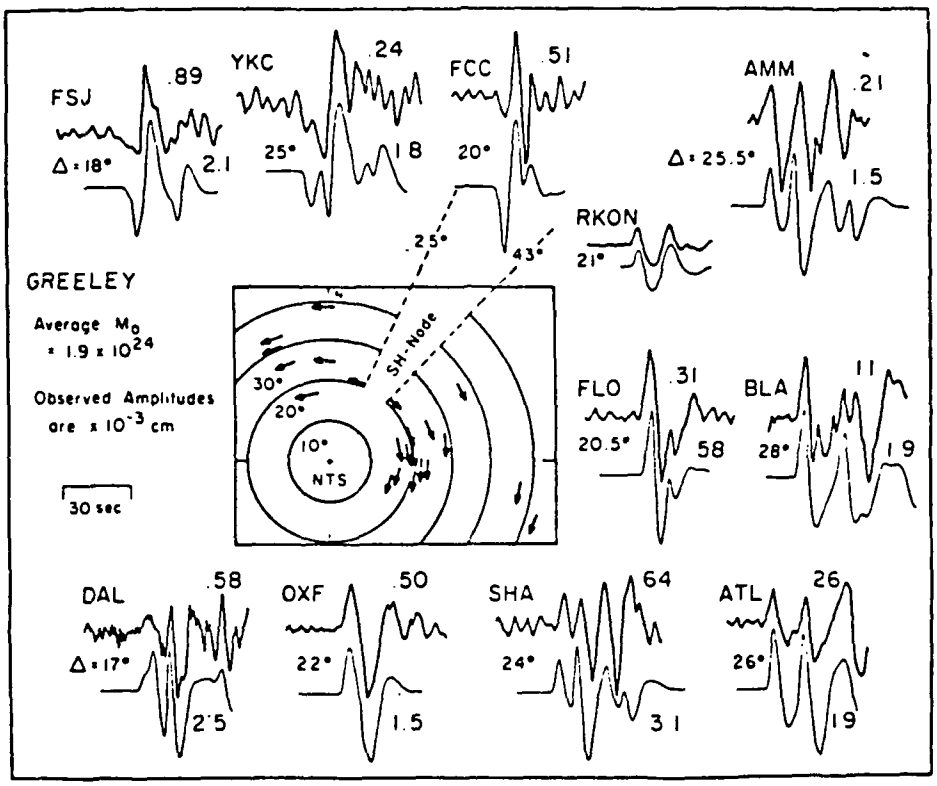

Figure II-6: A comparison of the SH waveforms from the explosion GREELEY with synthetics generated for a vertical strike-slip fault with the orientation consistent with Pahute Mesa tectonic release. The structure model used is laterally varying (see Helmberger et al., 1985). Above the observed SH pulse is the maximum amplitude in 10^{-3} cm, while the number below the synthetic is the moment required to produce the observed amplitude.

TABLE II-1

REVISED MOMENTS FOR TECTONIC RELEASE FROM PAHUTE MESA EXPLOSIONS

Name	Date (m-d-yr)	Origin Time	Lat. (°N)	Long. (°W)	Depth (km)	m_b	M_o X 10^{24}
Almendro	06-06-73	13:00	37.24	116.35	1.064	6.1	0.61
Benham	12-19-66	16:30	37.23	116.47	1.402	6.3	3.43
Boxcar	04-26-68	15:00	37.29	116.46	1.158	6.2	0.86
Camembert	06-26-75	12:30	37.28	116.37	1.311	6.1	0.86
Cheshire	02-14-76	11:30	37.24	116.47	1.167	5.8	0.43
Colby	03-14-75	12:30	37.31	116.47	1.273	6.2	0.49
Estuary	03-09-76	14:00	37.31	116.36	0.869	5.8	0.43
Fontina	02-12-76	14:45	37.27	116.49	1.219	6.1	1.35
Greeley	12-20-66	15:30	37.30	116.41	1.215	6.3	1.90
Halfbeak	06-30-66	22:15	37.32	116.30	0.819	6.1	0.61
Handley	03-26-70	19:00	37.30	116.53	1.206	6.4	1.47
Inlet	11-20-75	15:00	37.22	116.37	0.817	5.9	0.18
Jorum	09-16-69	14:30	37.31	116.46	1.158	6.1	0.31
Kusseri	10-28-75	14:30	37.29	116.41	1.265	6.2	1.22
Mast	06-19-75	13:00	37.35	116.32	0.912	5.9	0.31
Muenster	01-03-76	19:15	37.30	116.33	1.451	6.2	1.96
Pipkin	10-08-69	14:30	37.26	116.44	0.617	5.6	0.12
Pool	03-17-76	14:15	37.26	116.31	0.879	6.0	0.12
Scotch	05-23-67	14:00	37.27	116.37	0.978	5.7	0.18
Stilton	06-03-75	14:20	37.34	116.52	0.731	5.8	0.07
Tybo	05-14-75	14:00	37.22	116.47	0.765	5.9	0.18

m_b bias is to analyze large data sets, and attempt to model complexity such as Douglas et al.'s slapdown phase.

III. FREQUENCY DEPENDENCE OF TECTONIC RELEASE AT REGIONAL DISTANCES

At regional distances, seismograms are very complicated due to the waveguide nature of the crust. Wallace (1986) discusses the details of constructing synthetic seismograms in the distance range of 3° to 14°. The long-period P_{nl} wave forms for explosive sources are quite distinct from those of an earthquake. The absence of S in the source and the high-frequency time function result in seismograms that do not have well-developed PL phases. On the other hand, shallow earthquakes in the western U.S. with magnitudes greater than about 4.8 routinely write measurable, long-period PL phases at one or two WWSSN stations. Under favorable circumstances, it should be possible to separate the explosion and tectonic release effects. The biggest advantage to using regional distance records is that small events still produce large signal-to-noise ratio records in a fairly broad frequency band.

Certain systematic affects emerge when a large number of regional distance seismograms from Pahute Mesa explosions are compared. For example, the P_{nl} waveforms recorded at ALQ and TUC appear much more like those produced by earthquakes than by explosions. Figure III-1 is a composite of different explosions recorded at the regional WWSSN network. These long-period seismograms have been convolved with a filter whose impulse response is a triangle with a 2-sec rise and fall. Shown below the observations are a pair of synthetics which have been similarly filtered (the synthetics were generated with generalized rays and crustal model described in Wallace et al., 1982). These synthetics correspond to a pure explosion source and an earthquake source, respectively.

The earthquake source has a strike-slip mechanism described by Toksöz and Kehrer (1972); right-lateral motion on a plane striking N15°W. ALG and TUC are in the radiation lobe for the tectonic release P_{nl}, while LON, which is in good agreement with the explosion

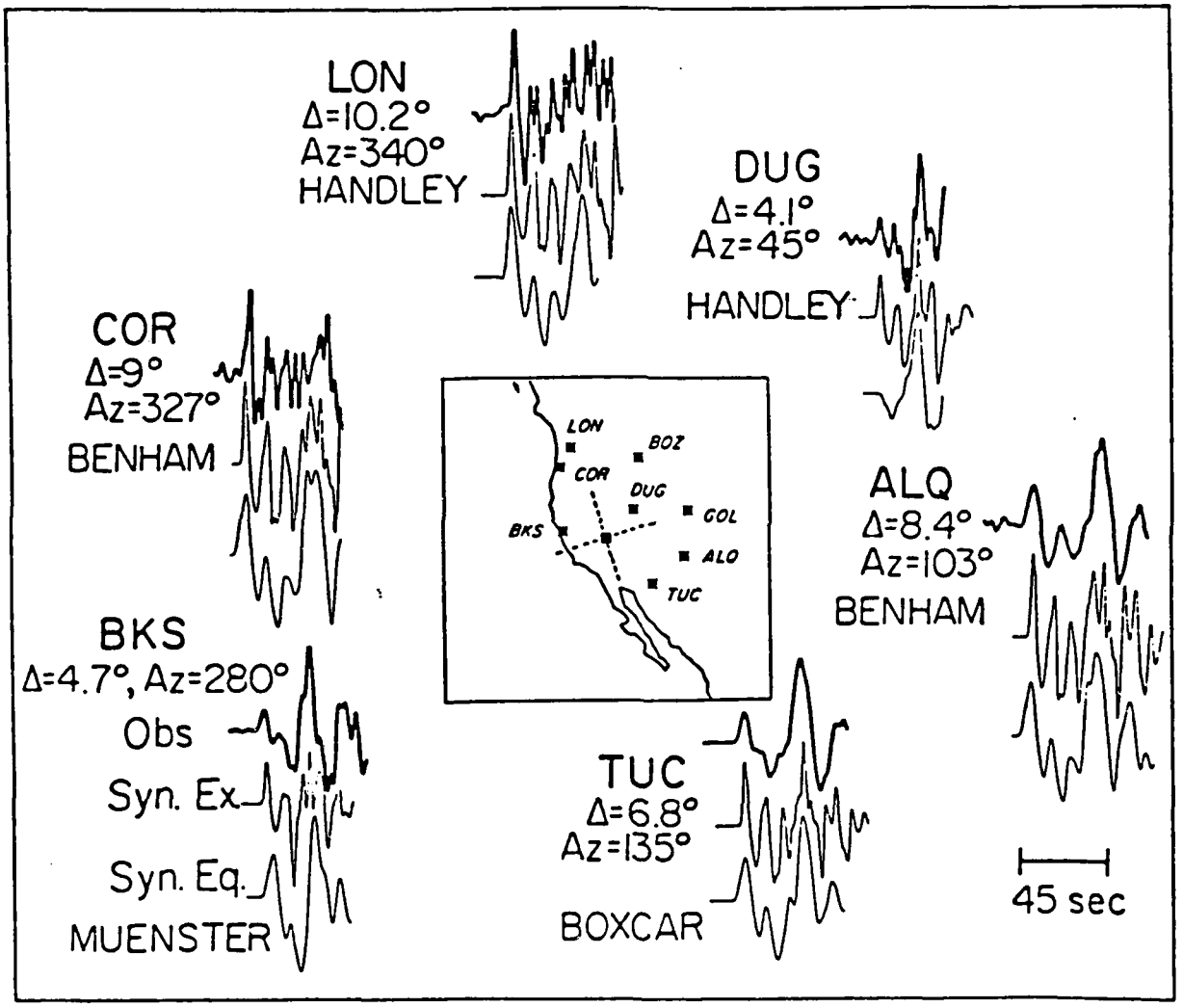

Figure III-1: The P_{nl} waveforms for several Pahute Mesa explosions (top trace at each station) and synthetics for an explosion source (middle trace) and a double couple (bottom trace). Both the observations and synthetics are lightly filtered. The fault orientation for the double couple is strike-slip; the nodal planes are sketched on the location map.

synthetic, is near a node. DUB, which is in the negative quadrant, has a greatly reduced P amplitude. Although Figure III-1 is a composite and no doubt the tectonic release varies from event to event, it is highly suggestive that there is significant tectonic release signature on P_{nl} waveforms.

FAULTLESS was detonated about 100 km north of Pahute Mesa at Hot Creek Valley, Nevada. In contrast to the Pahute explosions, the FAULTLESS P_{nl} waveforms show much less evidence of tectonic release associated with detonation (FAULTLESS does appear to have numerous strain release episodes 10 to 50 seconds after detonation, although they are very small). Figure III-2 shows the regional long-period records. Again the waveforms have been filtered as described in the previous paragraph. Shown below each observation is a synthetic for an explosion source. Although TUC is not fully explained by an explosion alone, the tectonic release must be down by a factor of 3 in comparison with GREELEY, or a factor of 1.5 in comparison with BOXCAR.

In an attempt to isolate the tectonic release signature on P_{nl} waveforms, synthetics were made in which a double couple was added to an explosion synthetic. The attempt here is to qualify the nature of tectonic release for the composite records shown in Figure III-1, so each record is fit independently, although the orientation of the double couple was constrained to be the same for all the records. The explosion synthetics were constructed using a source time function described by Helmberger and Hadley (1981). They used their source time function to model both near-in velocity records and far-field displacements for HANDLEY, one of the explosions considered in Figure 3; so the values they determined for rise time and overshoot ($k = 5$, $B = 2$) are assumed for all modeling. Changing the values of k and B within reasonable limits had little effect on the filtered synthetics. This is similarly true if we had used a Haskell (1967) or a Von Seggern and Bolandford (1972) source.

Strike-slip orientations have the largest effect on the P_{nl} waveforms for explosions. The displacement response from dip-slip faulting is higher frequency than that for strike-slip

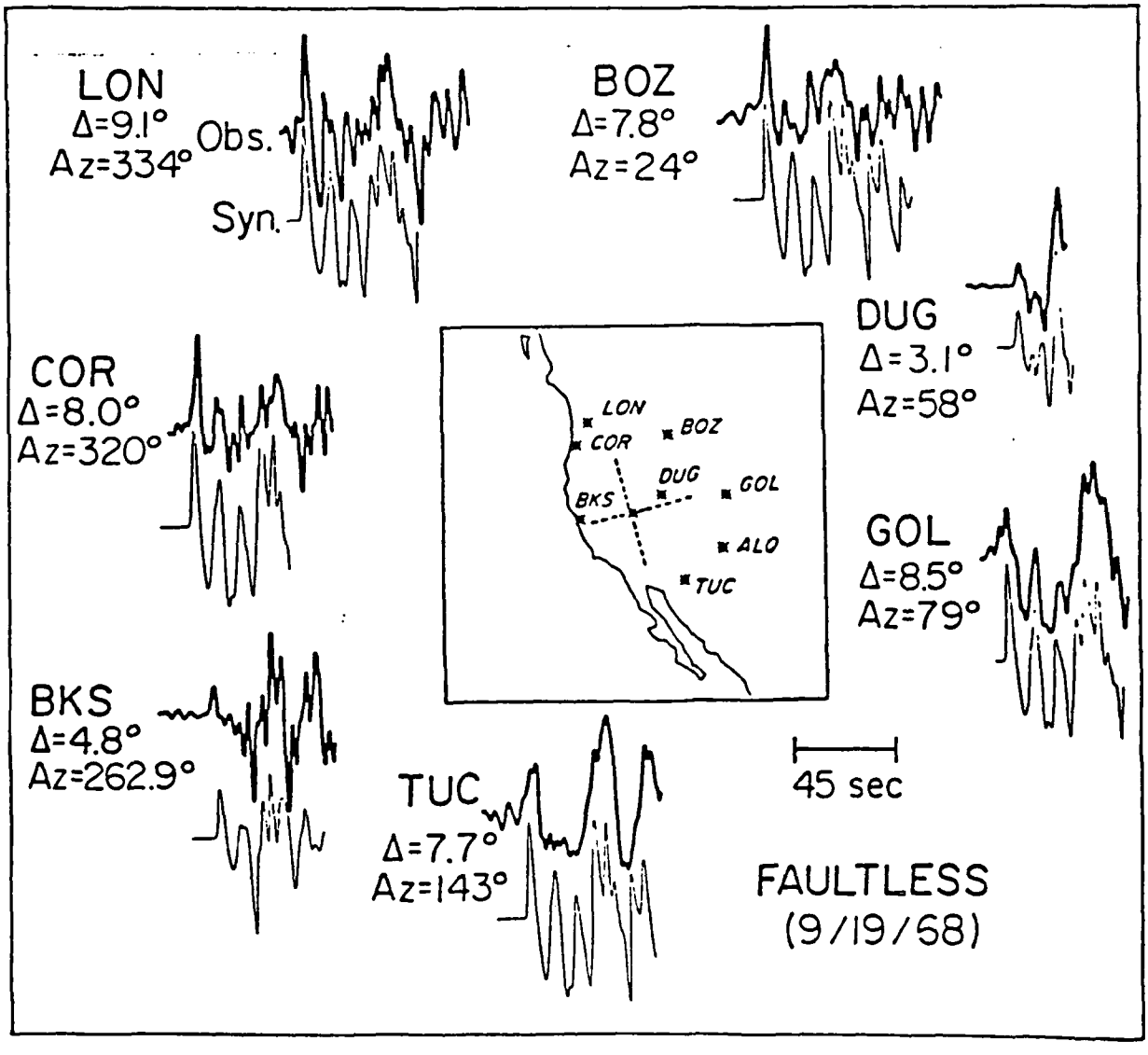

Figure III-2: A comparison of the P_{nl} waveforms for the explosion FAULTLESS (top trace) and synthetics computed for an explosion source. Both the observations and synthetics have been lightly filtered.

motion (this is a result of excitation) and generally adds or subtracts to the explosion waveform without substantially changing it. Since the ration of dip-slip to strike-slip motion is small on the basis of Wallace et al. (1984), only the orientation of the strike-slip component was determined. Different orientations for the strike were tested for compatibility with the observations. Figure III-3 summarizes the analysis. Shown are the same explosions as in Figure III-1, and synthetics generated for a combination of double couple and explosion.

The LON and COR records have a profound effect on the strike of the double couple. The contribution of the explosion to the waveform is much greater than that of the double couple, implying that these stations are near the node of the radiation pattern. This is particularly true of LON for nine different explosions. The best fitting strike-slip fault has a strike of N20°W (not significantly different from that of Toksöz and Kehrer (1972). The numbers to the right of each seismogram pair in Figure III-3 give the ratio of P_n displacement caused by the explosion contribution to that caused by the strike-slip dislocation. Since different explosions are used in the composite figure, no absolute moments are given. Rather, the ratios give a measure of the importance of tectonic release for a given azimuth.

Figure III-4 shows the vertical component for 12 Pahute explosion waveforms at PAS, a long-period (30-90) station 5.5° from NTS. At the periods of these records, it is assumed that the travel paths are identical, and most of the differences in the waveform must be due to source. It is interesting to compare events which are spatially very close but separated in time. For example, GREELEY (12-20-66) and KASSERI (10-28-75) are less than 3 km apart and about the same yield, but GREELEY has a much higher tectonic release. In Figure III-4 the PAS records are very similar, except that KASSERI is deficient in the long periods. Single station comparisons of many events should make it possible to develop an algorithm to identify source effects such as depth of burial as well as tectonic release.

It is a fairly straightforward process to invert for the moment tensor (MT) of a seismic source, provided adequate Green's functions can be constructed, although for shallow

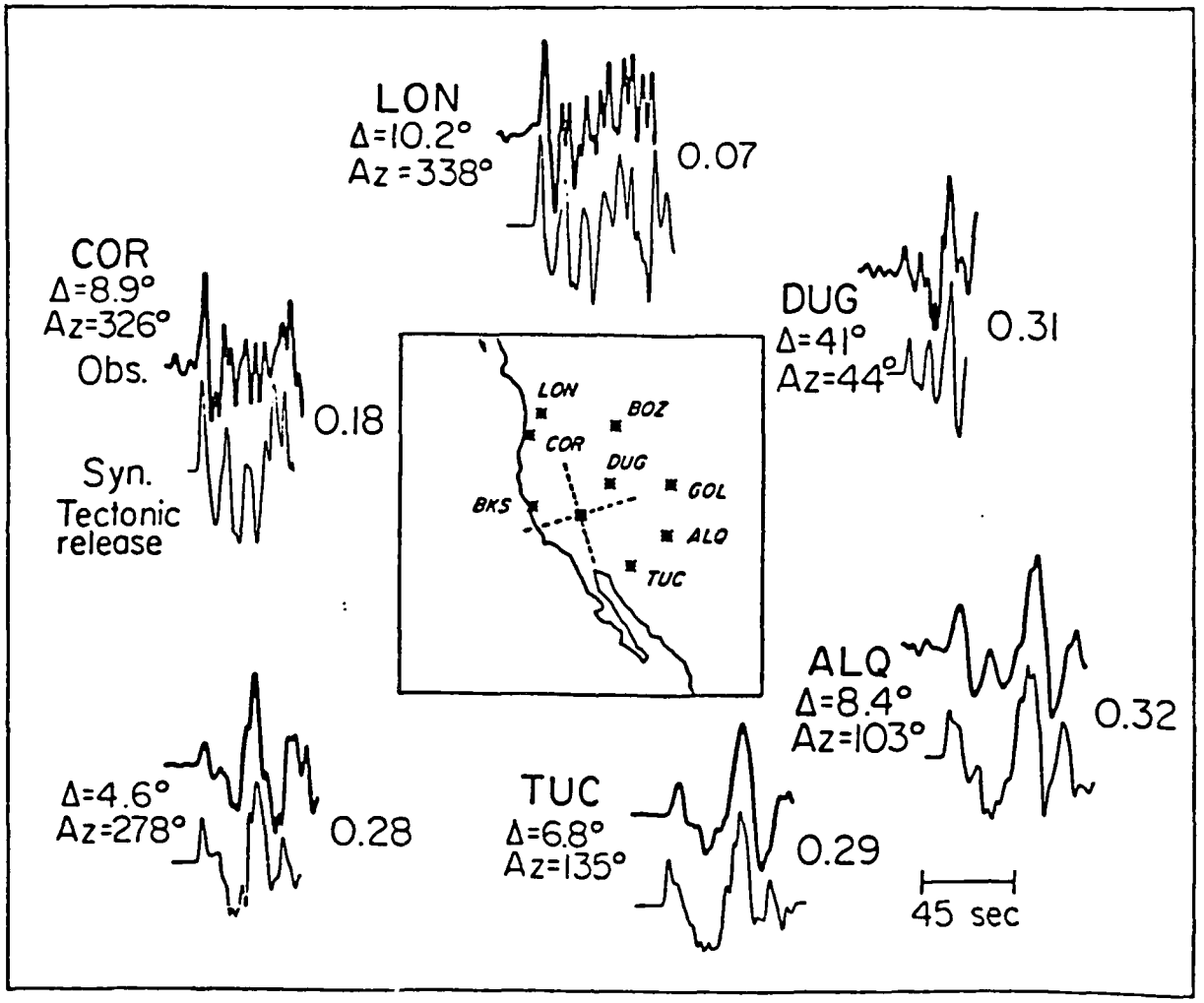

Figure III-3: A comparison of the P_{nl} waveforms of the same explosions as in Figure III-1 and synthetic explosion waveforms with a component of tectonic release. Both observations and synthetics have been lightly filtered. The numbers to the right of each seismogram pair give the ratio of Pn amplitude due to the double couple and that due to the explosion.

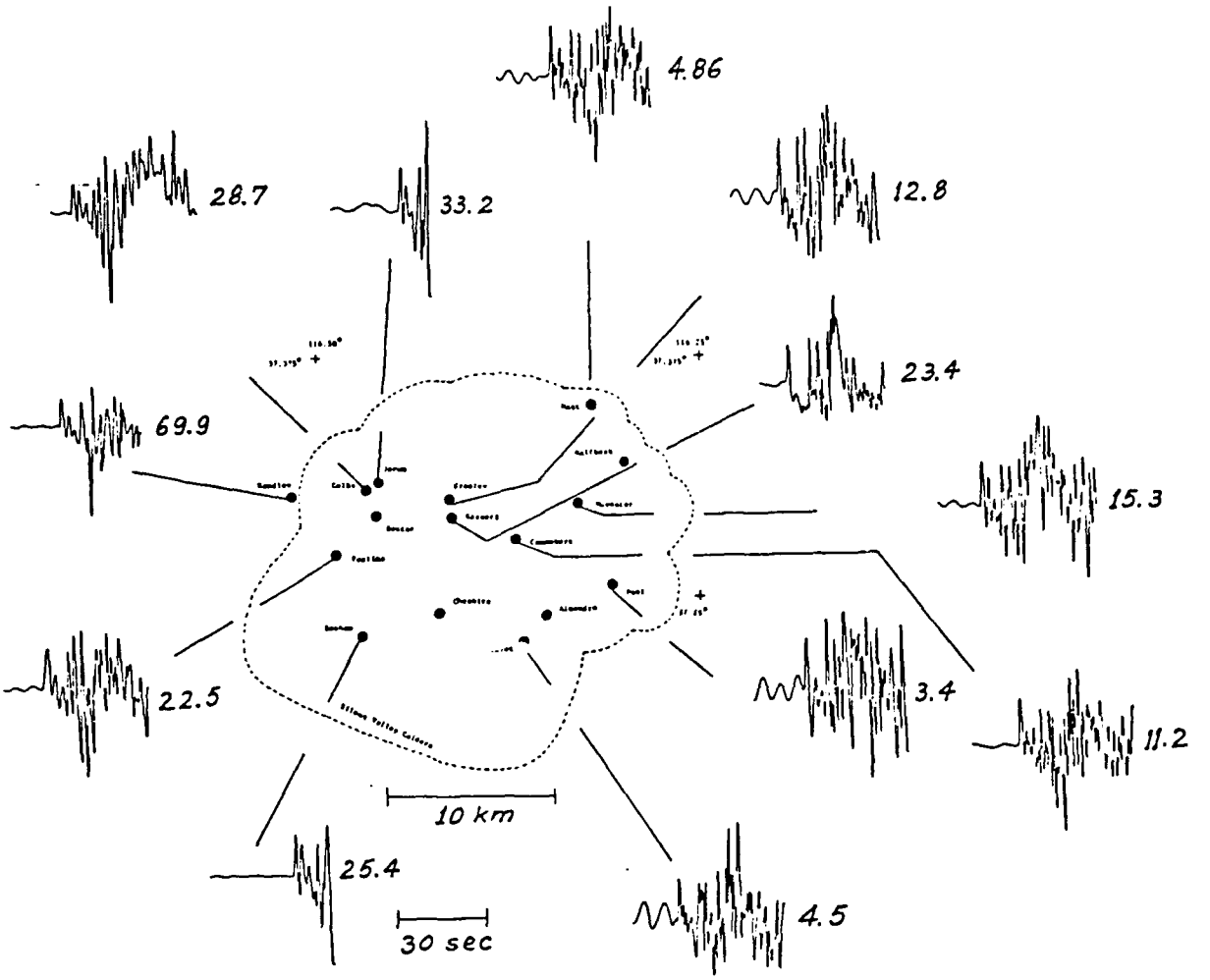

Figure III-4: Vertical seismograms for 12 Pahute Mesa explosions at PAS (30-90). The station is 3.3° from NTS. Numbers to right of traces give the maximum amplitude in mm.

explosions, high-frequency data are required to constrain the M_{zi} components. The explosion moment is the average of the trace of the moment tensor, and the deviatoric component is the remainder. We have inverted the regional body waves recorded on the broadband Lawrence Livermore National Laboratory network for three Pahute Mesa explosions (CHESIRE, FARM and POOL) in different frequency bands in an attempt to isolate any frequency dependence of the deviatoric component of the MT.

At long periods (>2 seconds) a two-layered crust over a halfspace mantle was a sufficient travel path structure to recover the moment tensor. Table III-1 shows the isotropic and major double couple components of the MT. Also shown is the size of the minor double couple, an indication of the likelihood that the major double couple actually represents tectonic release. The inversion was performed in a linear fashion, which requires that all the elements of the MT have the same time history. It was assumed that the explosion had a Helmberger-Hadley time history with k = 15, B = 0. Although this is a poor representation for the tectonic release time history, it is probably sufficient considering the uncertainty in the travel path structure.

Figure III-5 shows the frequency dependence of the deviatoric part of the moment tensor for the three NTS events. The LLNL records were band-pass filtered (the high-frequency cut-off is shown on the abscissa). The resulting moment tensor had the long-period isotropic component subtracted from it, and the largest remaining eigenvalue was assumed to represent the tectonic release (the direction of stress axes was not considered). As can be seen, the apparent size of the tectonic release decreases with increasing frequency. It is difficult to explain the frequency dependence of the tectonic release. At long periods, the regional-distance data is consistent with the teleseismic analysis.

Murphy et al. (1986) studied the m_b anomaly associated with the RULISON explosion (10 September 1969, yield 40 kt). The observed m_b is up to 0.3 units smaller than expected based on a comparison with GASBUGGY. Murphy et al. attribute this anomaly to the signature of

TABLE III-1

MOMENT TENSOR INVERSION RESULTS

Event	Date	M_{ex} (dyne-cm)	M_{dc}	M_{mdc}
FARM	9-13-80	.01 X 10_{24}	.003	.002
CHESHIRE	2-14-76	.67 X 10_{24}	.36	.07
POOL	3-17-76	.42 X 10_{24}	.19	.12

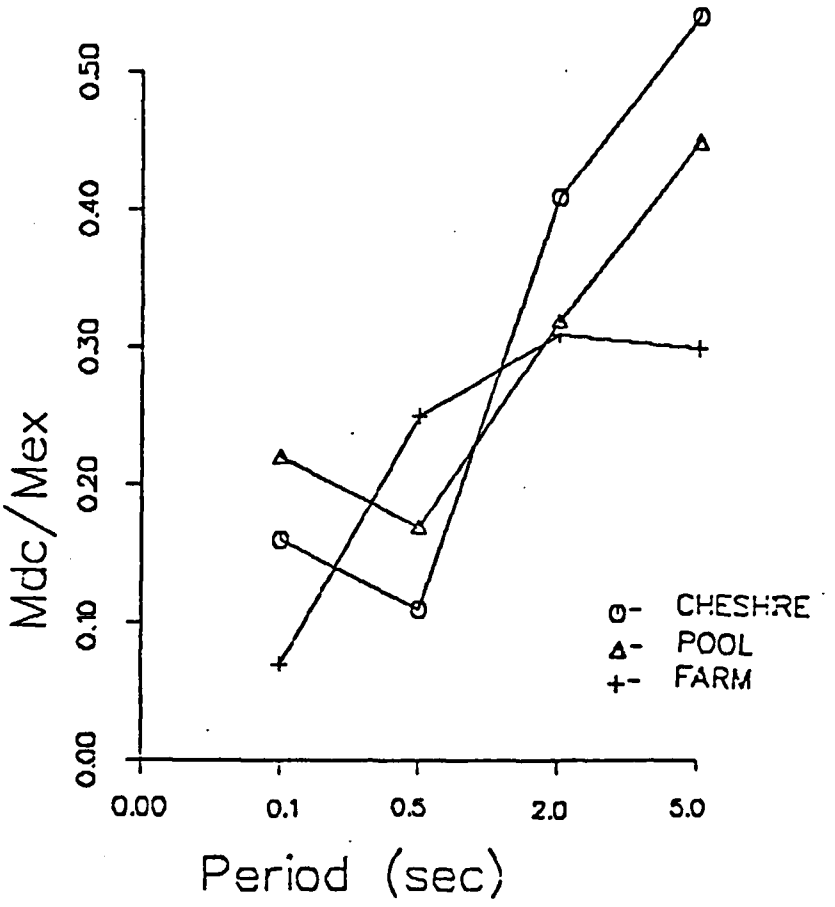

Figure III-5: The ratio of the deviatoric to explosion moment for Pahute Mesa explosions CHESHIRE, POOL and FARM. M_{ex} is only determined at long periods.

tectonic release. In this case, the tectonic release orientation is a normal fault, so it subtracts from the compressional P wave arrivals. Murphy et al. attribute this anomaly to the signature of tectonic release. In this case, the tectonic release orientation is a normal fault, so it subtracts from the compressional P wave arrivals. Murphy et al. further state that the amplitude of the vertical component Lg is affected by the tectonic release, thus still providing a good yield estimator.

VI. NEAR-FIELD TECTONIC RELEASE

The tangential motions recorded in the near-field from underground nuclear explosions are inconsistent with the teleseismic representation of the tectonic release. As an example of this, Figure VI-1 shows the three components of ground motion from BOXCAR recorded at a distance of 7.4 km. Also shown in Figure VI-1 are synthetics for an explosion source function and a double couple. The velocity structure that was used for the synthetics is that determined by Barker et al. (1985). The P wave arrivals are matched to first order by the explosion synthetic. The SH waves were generated using a moment of 0.86 X 10^{24} dyne-cm (Wallace et al., 1986). As can be seen, the tangential component is poorly matched. This gross mismatch indicates two things: (1) significant off-azimuth energy, and (2) the inadequacy of a point source representation for the tectonic release. On the basis of our teleseismic modeling of the SH energy from nuclear explosions, we would argue strongly that there is appreciable release of tectonic strain, and that the tangential energy is not a product of asymmetry of the explosion source (see Wallace et al., 1985, 1986). If the tectonic release is purely a triggered fault motion as suggested by Aki and Tsaiu (1972), then it would be expected that the strong-motion SH waves would be similar to those produced by a similar-sized earthquake. Figure VI-2 compares the SH waves from an aftershock of the 1979 Imperial Valley earthquake (Ml = 5.0, Mo = 0.7 X 10^{24} dyne-cm) recorded at 10.4 km distance with the BOXCAR record and a synthetic for a simple dislocation model. Apparently, the point source representation is sufficient for the earthquake, implying that at least some component of the tangential record from the explosion is due to a mechanism other than triggered fault motion.

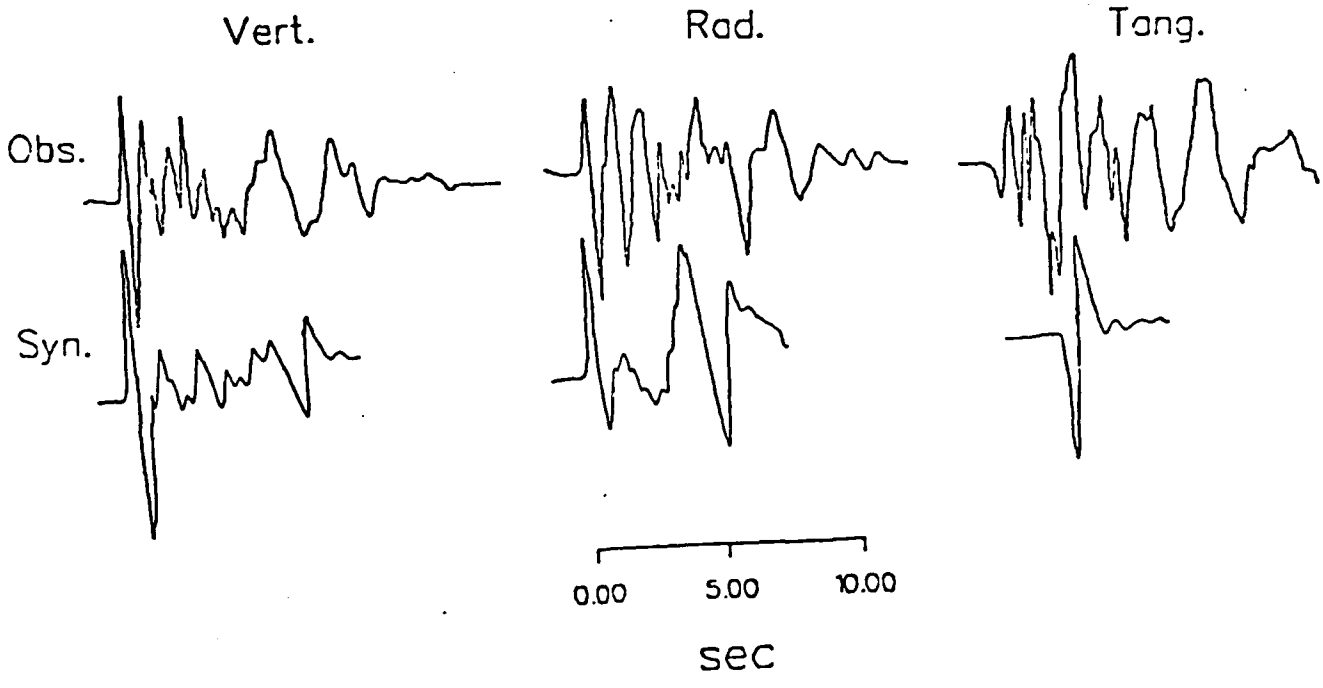

Figure IV-1: Comparison of strong ground motion from BOXCAR observed at a recording site 7.4 km away from the source with synthetic seismograms calculated using the model of Hartzell et al. (1983). The tangential model is from the best fitting point-source double couple.

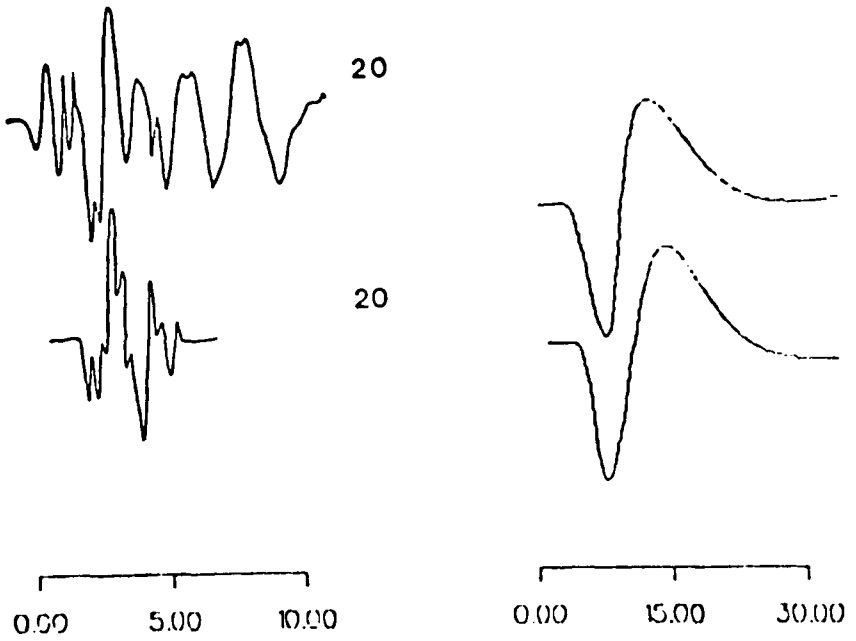

Figure IV-3: Distributed source SH waves in the near and far field. The strong motion fit requires a total moment of 0.38×10^{24} dyne-cm. The far-field comparison is for a single point source with a moment of 0.38×10^{24} and 16 sources of 0.22×10^{23} dyne-cm. There is no difference in waveform or amplitude.

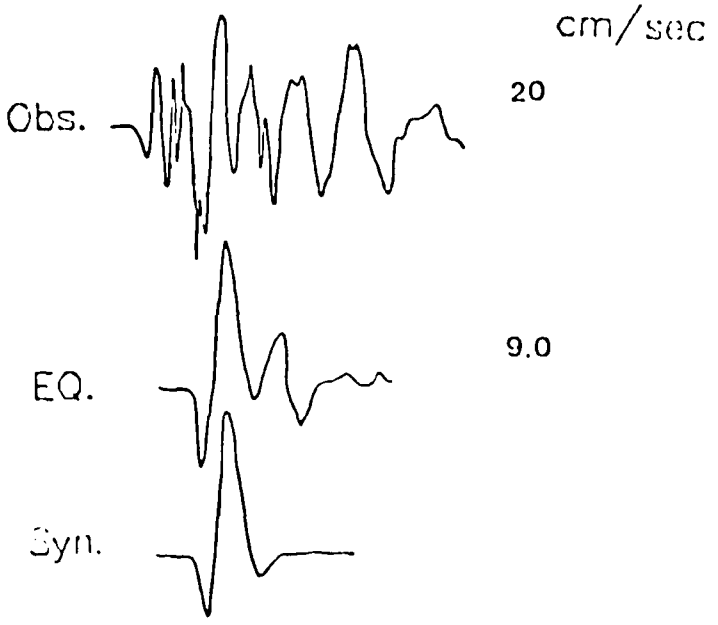

Figure IV-2: Comparison of BOXCAR and an Imperial Valley aftershock with a synthetic SH wavetrain. The explosion and earthquake have approximately the same far-field moment.

Archambeau (1972) proposed a mechanism for tectonic release which is due to the loss of strength of the material in a volume about the explosion. In an attempt to simulate this model, we constructed a spherical, symmetric, distributed source. We placed 16 point sources (of equal moment) about the working point. The elastic radius, or extent of shear stress drop, expected for Archambeau's model is given by:

$$R_e = F\rho\alpha^3\psi(\infty)\ \Delta\sigma$$

where F is the ratio of the tectonic release moment to the explosion moment, $\Delta\sigma$ is the stress drop, ρ and α are the source region density and P velocity, respectively, and $\psi(\infty)$ is the static level of the explosion displacement potential. For BOXCAR (1000 kt) and the F factor calculated on the basis of the tectonic release moment of 0.87 X 10^{24} dyne-cm, the elastic radius should be on the order of 1.1 km if the stress drop is 100 bars. This radius seems extraordinarily large, and indeed would have a significant effect on a recording only 7 km away. The value of 100 bars for stress drop is taken from the "average" intraplate earthquake (Liu and Kanamori, 1983). For earlier work (Wallace et al., 1983), it was shown that the sP waveforms from BOXCAR required a much higher stress drop: 30-500 bars. This is consistent with the work of McKeown and Dickey (1969), who showed that the aftershock distribution of explosions with large F factors is confined to a region much smaller than expected for an earthquake of comparable moment. Using a stress drop of 500 bars, the elastic radius for BOXCAR is 0.3 km. We used this radius to define the sphere of the distributed source.

Figure IV-3 shows a comparison of the observed tangential and distributed source synthetic waveforms for BOXCAR. Although the match is not perfect, it does preserve the character of the interference pattern. Also shown in Figure IV-3 is the long-period teleseismic SH pulse from the distributed source compared with that from a point source. It is apparent that the distributed source model will satisfy the local data and far-field observation, although the seismic moment that is required in the near field is one half that derived on the basis of teleseismic data alone.

One of the main problems in dealing with the near-field data is the poor azimuthal and range coverage. It is difficult to see coherence in the SH pulse or node changes. One exception appears to be HALFBEAK (30 June 1966, yield 300 kt). This event has a large F factor (1.9, using the moment determined by Wallace et al., 1986) and has very coherent SH arrivals in the near field. Figure IV-4 shows the tangential components arranged in distance from 0.91 to 3.0 km. Stations 4, 5, and 6 are in a line striking north of HALFBEAK. This line of stations is along a direction predicted to be a maximum for the tectonic release SH (on the basis of the teleseismic modeling). Station S8 is to the east, and is predicted to have a polarity reversal as compared to S6. On the basis of timing, this reversal can be seen, although it is not as dramatic as expected.

Figure IV-5 shows the tangential recordings from HALFBEAK and synthetics generated for a distributed shear dislocation source. The velocity structure that was used for the synthetics is that determined by Barker et al. (1985). Green's functions were computed with Kennet-Bouchen numerical integration. The source orientation for the shear dislocations was determined by a constrained moment tensor inversion. It was assumed that the orientation was strike-slip, and the tangential waveforms were inverted for strike. The resulting value, θ = N7°E, is consistent with larger Pahute Mesa events studied teleseismically (Wallace et al., 1985, 1986). The inversion produced a stable estimate of strike, but the quality of fit to the waveforms was quite poor. Since the near-field recordings are only 2-4 times the depth of burial (d = 815 m), tectonic release from a distributed source will produce a very complicated interference pattern. In an attempt to simulate this effect, we placed 16 point sources (of equal moment, the total of which was determined by the moment tensor inversion) about the working point at the distance of 1 elastic radius (given by Archambeau, 1972, and a stress drop of 100 bars). Although the fit in Figure IV-5 is not perfect, it does offer a reasonable explanation for the data. In the next step, we plan to use this model for tectonic release to fit the vertical and radial near-field observations.

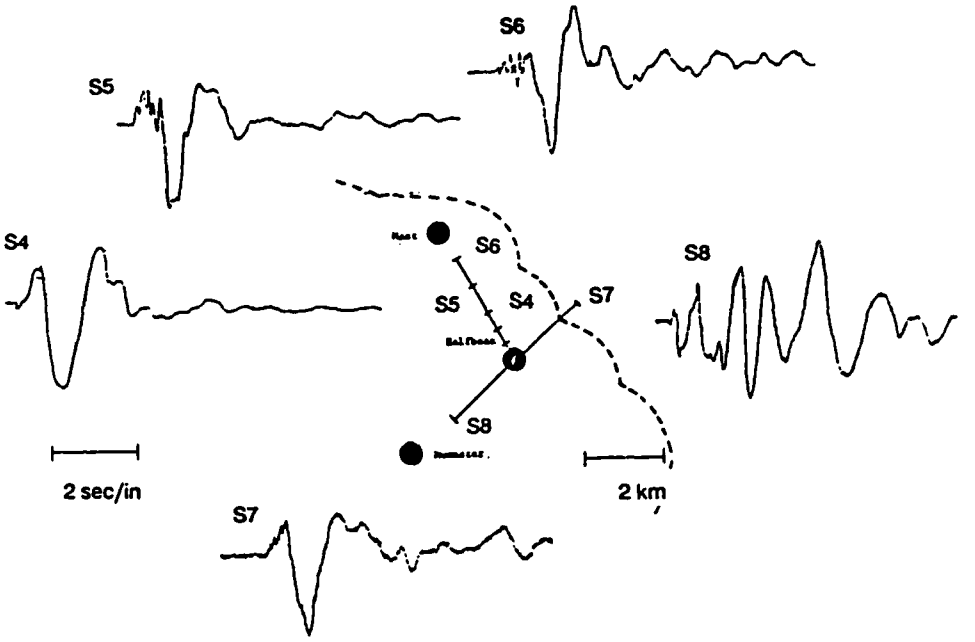

Figure IV-4: Tangential Displacements for HALFBEAK. Dashed outline is the Silent Canyon Caldera. The S4-S6 profile is near the SH max.

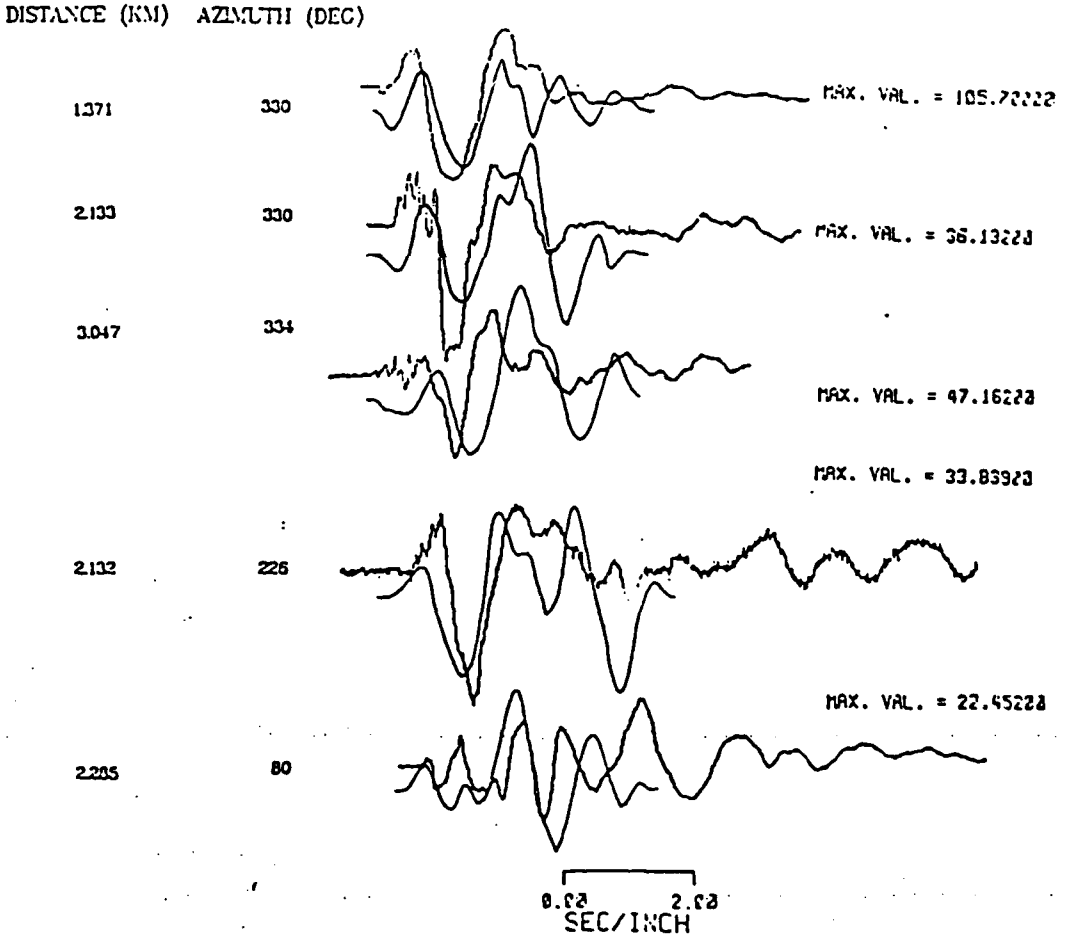

Figure IV-5: A comparison of the observed and synthetic near-field records from HALFBEAK. Top trace is the observed velocity. The synthetics were calculated with a distributed shear dislocation source.

V. JOINT INVERSION OF REGIONAL AND TELESEISMIC WAVEFORMS

The inconsistency of data from different distances makes the absolute determination of tectonic release source parameters suspect. Any tectonic release model must explain the discrepancy between regional and teleseismic estimates of the tectonic release size. Unfortunately, many explosions contain only a few usable teleseismic records, so in general we are dealing with a sparse data set. We have developed a procedure for the joint inversion of regional and teleseismic long-period waveforms for source parameter estimates. At present, the procedure has only been used on earthquake waveforms.

The source parameters of moderate to large-sized earthquakes are widely used to inter the present day tectonic environment. In most regions, large earthquakes are infrequent, and moderate-sized events must be used to investigate the style of deformation and state of stress. Unfortunately, useful recordings of moderate-sized events at teleseismic distances are often sparse, making it difficult to constrain the source mechanism through the inversion of teleseismic long-period body waves alone. Wallace et al. (1981) introduced a method for the determination of source parameters by the inversion of regional-distance long-period body waves. This method has proved valuable, and as little as three stations (azimuthally distributed) are required in order to constrain a solution. The reason for this is the nature of Pn_l wave trains: the combination of P and SV rays provides a greater coverage of the outer portion of the focal sphere than teleseismic P and SH waves, which have much steeper take-off angles. In addition, as much as 90 seconds of record can be fit in regional waveform inversions, whereas most useful information from shallow-source mechanisms occurs in the first 30 seconds of the teleseismic waveform. On the other hand, regional waveforms are relatively insensitive to source depth, and teleseismic information can be used to constrain this

parameter. Ideally, a method which inverts both of these data simultaneously will provide the best constraints on source parameters. A joint inversion of teleseismic P and SH, and regional vertical and radial component long-period waveforms, has the distinct advantage of examining energy with take-off angles that range from 18°-52°, considerably better coverage than teleseismic waveform or regional waveform inversion alone. This paper presents a technique for the simultaneous inversion of teleseismic and regional long-period waveforms for source parameters. The utility and benefits of the inversion method will be demonstrated on synthetically derived data for three cases.

The Forward Model

The teleseismic and regional P and S wave synthetics can be expressed in cylindrical coordinates as

$$Wp(r,z,\theta,t) = M_o/4\pi\rho_0(S(t)^* \sum_{i=1}^{3} G_i(t)A_i)$$

$$Wx(r,z,\theta,t) = M_o/4\pi\rho_0(S(t)^* \sum_{j=1}^{2} G_j(t)A_{j+3})$$

where wp and Ws are the P wave and SH wave displacements, respectively, M_o is the seismic moment, ρ_0 is the source region density, and S(t) is the far-field time history. The A_i's are the source coefficients determined by source orientation:

$$A_1(\theta,\lambda,\delta) = \sin 2\theta \cos\lambda \sin\delta + (1/2)\cos 2\theta \sin\lambda \sin 2\delta$$

$$A_2(\theta,\lambda,\delta) = \cos\theta \cos\lambda \cos\delta - \sin\theta \sin\lambda \cos 2\delta$$

$$A_3(\theta,\lambda,\delta) = (1/2)\sin\lambda \sin 2\theta$$

where θ is the receiver azimuth from the end of the fault plane, λ is the rake angle, and δ is the dip angle.

The G_i terms represent the Green's functions for the three fundamental faults; G_1 = vertical strike-slip, G_2 = vertical dip-slip, and G_3 = 45 dip-slip. The Green's functions for the regional distance are for either the vertical or radial component and were generated using generalized ray theory.

The Method of Inversion

We employed the inversion method described by Wallace et al. (1981), which uses the error function

$$e = 1 - \int fg/(\int f^2)^{1/2}(\int g^2)^{1/2} \quad (1),$$

where f is the observed record and g is the synthetic waveform. There is an error associated with each waveform observation and the sum of the squares of these errors can be minimized with respect to the three fault parameters strike, dip, and rake (θ, δ and λ) through an iterative nonlinear inversion. The generalized inverse for this inversion can be expressed in the form of singular value decomposition (SVD) as $V_p\Lambda^{-1}_pU_p$, where V_p is a p X p matrix of model eigenvectors v_i (p = number of nonzero single values) and Up is a N X p matrix of data eigenvectors u_i (N = number of observations). The term Λ^{-1}_p is a p X p matrix composed of diagonal elements of the form $1/\lambda_i$, where λ_i are the eigenvalues or single values. The model parameter vector change can thus be expressed as the weighted sum of the model eigenvectors as $\sum_{i=1}^{P} a_iv_i$, where

$$a_i = 1/\lambda_i u_i^T e \quad (2).$$

One benefit of SVD is that the influence a single station or set of stations are having on the model parameter estimates can be easily determined. To increase stability in the nonlinear inversion, a damping factor can be included so that the generalized inverse is in the form V_p diag$(\lambda_i/\lambda_i^2 + \beta)U_p^T$, where β is the damping factor. This takes care of the problem of small single values, which can cause unusually large changes in the model parameter estimates during the iteration process. The maximum likelihood inverse or weighted least-squares can also be used when it can be determined that noisy observations are imposing a strong influence on the model parameter estimates.

Results

Three test cases were studied to illustrate the strengths of joint inversion of regional and teleseismic data. The first case is a pure strike-slip mechanism shown in Figure V-1.

There were eight teleseismic observations (four P wave and four SH) and four regional stations with vertical and radial components from each. The synthetic data were derived using a source depth of 10 km. Both the synthetic data and the Green's functions for the teleseismic distances were generated using the three rays, P, pP and sP. The starting solution was a pure normal fault (θ = 130°, δ = 45°, and λ = -90°). Figure V-1 shows the solution at 3, 6 and 10 iterations. The exact solution was obtained after 12 iterations. Also shown in Figure V-1 is a plot of the error function values from each inversion versus the Green's function source depth. A minimum error of zero was obtained using the 10-km Green's functions, thus constraining the source depth exactly.

Table V-1 contains the results for the same problem except that an inappropriate time function was used. Table I lists the solutions from each inversion using Green's functions generated for depths between 5-16 km. These results indicate that the inversion for model parameter estimates is robust for Green's function depths of 6-12 km, with strike, dip and rake only deviating from the true solution by 1°-3°. The error functions were minimized at 7 km (true depth = 10 km). Therefore, the time function does not strongly influence the model parameter estimates strike, dip and rake in the simultaneous inversion; however, it does influence the depth estimate. In this example, the long time function produced an underestimation of the source depth.

The next case addresses the problem of inadequate Green's functions. This case has the same station distribution as the previous example. The teleseismic synthetic data were generated using 13 rays, which consisted of many combinations of crustal bounces. The effects of a complicated receiver structure, which had 50 rays with many combinations of crustal reverberations and P-SV conversions in a 5-layer crust, were also included. The effects of P-SV conversions on the vertical component are small due to the steep ray path for teleseismic P-wave energy.

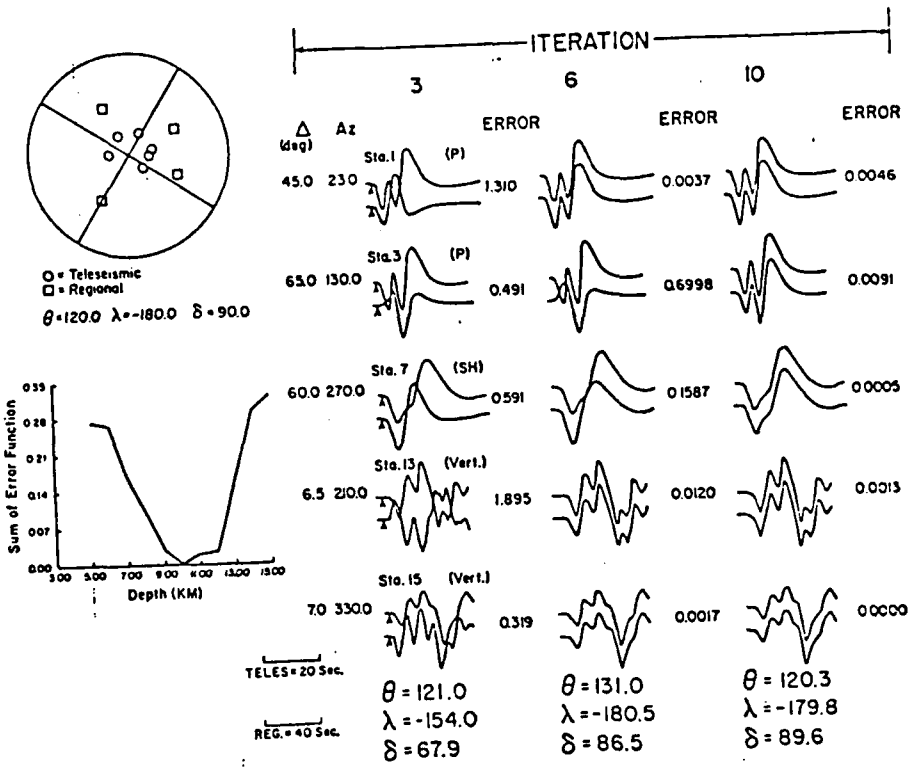

Figure V-1: Source mechanism and waveform fits at 3, 6, and 10 iterations. The error (equation 1) is next to each waveform (not all waveforms used in the inversion are shown). The synthetic observed waveform is on top, and the synthetic predicted waveform is on the bottom. The error for solutions obtained using different source depths is also shown. True source depth was 10 km.

TABLE V-1

INVERSION RESULTS USING SUITE OF GREEN'S FUNCTIONS AND AN INAPPROPRIATE TIME FUNCTION[a]

Depth (km)	Error[b]	Strike	Dip	Rake
5	.2344	211.6	88.5	2.5
6	.2037	34.6	89.6	-2.0
7	.1271	30.7	88.4	-0.7
9	.2159	32.5	88.9	-3.2
10	.2093	32.6	86.7	-0.6
11	.3374	30.7	85.6	-3.0
12	.2410	30.8	86.4	2.3
14	.4914	30.7	75.8	10.9
16	.4745	41.8	71.0	3.6

[a]Observed synthetic data had a trapezoid time function with rise time, rupture time, and fall time = 1, 2, 1.

[b]Average size of the error for all observations. Error is defined in equation 1 in text.

The results of the inversion using teleseismic data alone for this oblique-slip case are shown in Figure V-2a. Again, the teleseismic Green's functions were generated using only 3 rays and, therefore, are inadequate to completely model the observations. The true depth was 10 km, but the error functions were minimized using Green's functions generated for a 6-km depth. Table V-2 summarizes the source parameters obtained from the inversion using the suite of Green's functions. The error forms a broad minimum between 6 and 9 km. Therefore, the source depth from this inversion is poorly constrained. The solution from the teleseismic data alone (θ = 60°, δ = 50°, λ = 66°) is significantly different from the true solution, yet the waveform fits look very reasonable.

Figure V-2b shows the inversion results when the regional waveforms are included. The regional distance synthetic data for this example were generated using a crustal thickness of 30 km. The Green's functions were generated using a crustal thickness of 40 km and are, therefore, also inadequate. The inclusion of the regional waveforms in the inversion, however, had a significant effect on constraining the predicted solution to the true solution, even though the regional distance Green's functions are inadequate. Table V-3 shows the results of including the regional waveforms in the inversion. For all depths, although the size of the error might change, the model parameter estimates are within 1°-5° of the true solution. The addition of regional waveforms to the data set, therefore, has a significant stabilizing effect on the inversion. This result demonstrates the robustness of the regional distance Green's functions and is consistent with the findings of Wallace (1986) that regional distance waveforms are relatively insensitive to the fine details of crustal structure and crustal thickness, thus making them ideal for source parameter studies.

The teleseismic distance station distribution (seven P waves and four SH) and the pure normal mechanism of the third case are shown in Figure V-3a. This example suffers from poor teleseismic azimuthal coverage, a typical problem encountered for moderate-sized events. With the teleseismic data alone, the inversion suffered from nonuniqueness and instability from

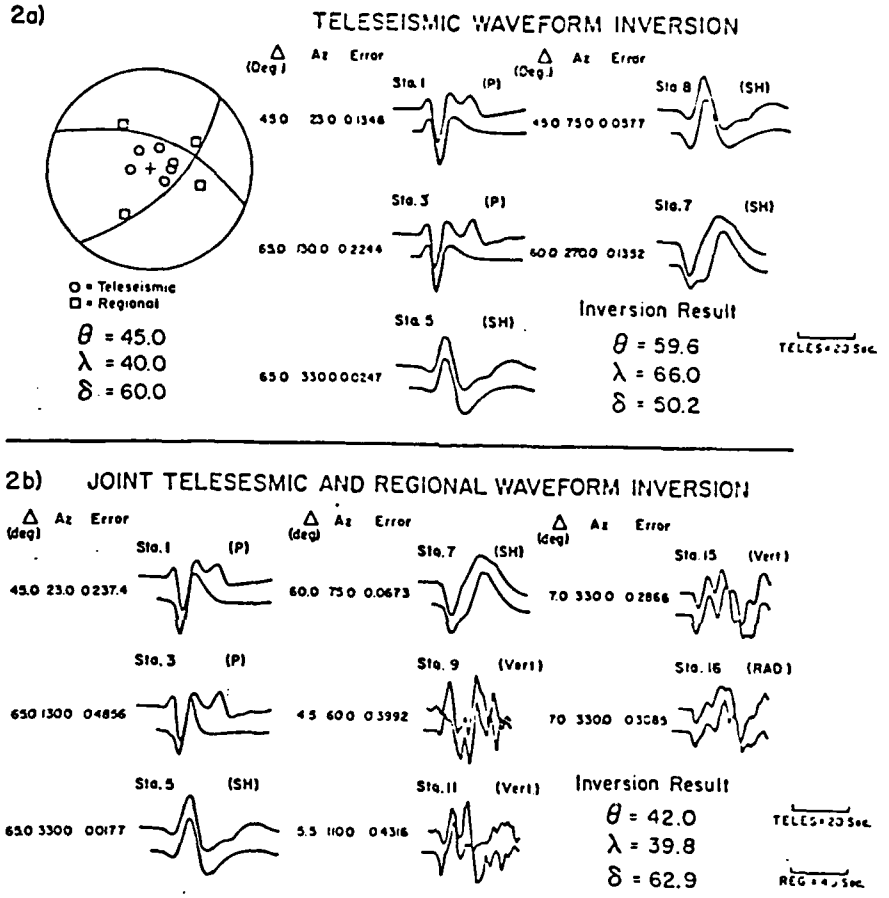

Figure V-2a: Inversion results from teleseismic data alone using inadequate teleseismic Green's functions. Note the acceptable waveform fits with a solution that deviates significantly from the true mechanism.

Figure V-2b: Results from joint inversion of teleseismic and regional waveforms. Regional waveforms were added to the teleseismic data set from Figure V-2a. Both teleseismic and regional distance Green's functions were inadequate. The inclusion of the regional data in the inversion produced a solution very close to the true mechanism, even though the regional distance Green's functions are inadequate. Stations 1 and 3 are near a nodal.

TABLE V-2

INVERSION RESULTS, TELESEISMIC DATA ALONE,
USING SUITE OF INADEQUATE GREEN'S FUNCTIONS

Depth (km)	Error	Strike	Dip	Rake
5	.4582	80.7	45.3	80.4
6	.2120	59.6	50.2	66.0
7	.2199	59.7	50.0	64.3
8	.2419	62.7	49.2	68.1
9	.2950	61.6	49.7	66.5
10	.3339	60.7	49.6	64.3
11	.5273	31.4	88.8	7.5
12	.6486	40.0	71.7	10.4
14	.5200	292.0	54.3	133.0
16	.6211	283.1	50.3	131.9

TABLE V-3

INVERSION RESULTS FOR BOTH TELESEISMIC AND REGIONAL DATA USING INADEQUATE GREEN'S FUNCTIONS

Depth (km)	Error	Strike	Dip	Rake
5	.5120	46.2	60.1	42.5
6	.3826	42.9	60.1	42.0
7	.3633	43.0	60.9	41.2
9	.3630	41.9	62.9	39.7
10	.3720	41.7	62.4	39.0
11	.3894	40.8	64.3	38.7
12	.3983	42.0	64.3	38.1
14	.4546	38.7	63.6	38.0
16	.5111	38.6	63.3	39.0

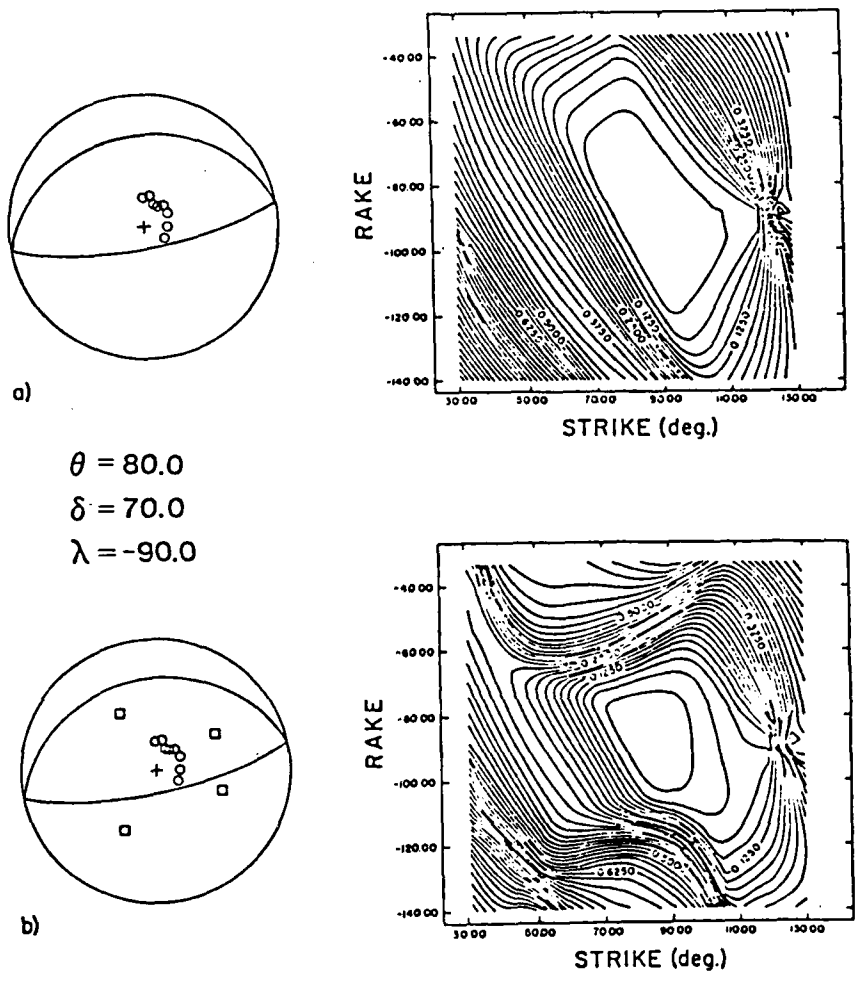

Figure V-3a: Solution space for pure normal fault mechanism with poor station distribution. The average size of the error function is contoured over the variation of strike and rake while dip is held constant at 70°. Elongated flat low-misfit region around true solution indicates a poorly resolved mechanism.

Figure V-3b: Solution space for normal fault after adding four regional stations (boxes). Mechanism is much better constrained and elongated flat region has disappeared.

small eigenvalues. Using a damping factor of 0.1 and a starting solution close to the true solution (θ = 40°, δ = 70°, λ = -90°), the inversion arrived at a nonunique solution (θ = -48°, δ = 25°, λ = -52°). Using a much larger constant damping factor of 3.0, the solution did not deviate far from the true solution; however, after 75 iterations, the parameter estimates (θ = 65°, δ = 61°, λ = -81°) had still failed to converge to the correct solution. The reason for this behavior can be seen in Figure V-3a. This figure shows the solution space for this problem. The average length of the error function is contoured over the variation of strike and rake while dip is held constant at 70°. An elongated trough forms a region of low misfit. The true solution lies close to the center of this trough, which explains the slow convergence and indicates nonuniqueness (anywhere in this region the solution is satisfactory).

With the addition of data from the four regional stations, the elongated trough in solution space has disappeared (Figure V-3b), and the region of low misfit covers a much smaller area. The added stability from the regional data is also observable in the inversion. Using a damping factor of 0.1, a solution of θ = 82°, δ = 68°, λ = -89° was obtained in 10 iterations (exact solution: θ = 80°, δ = 70°, λ = -90°).

In summary, these test cases have shown that the addition of regional waveforms to the set of observations provides a valuable constraint for the inversion of model parameter estimates and stabilizes the inversion process.

Advantages of SVD

A final example here demonstrates the insight that SVD provides. This example is identical to that shown in Figure V-3b, except that noise was added to the radial component of the regional waveform at station 12. With only one noisy observation, the final model parameter estimates were θ = 92°, δ = 68°, and λ = -105°. Thus, dip was unaffected by the noisy observation, but strike and rake deviate by as much as 15° from the correct values. An examination of the eigenvectors and eigenvalues reveal why this observation is having such a profound influence on the strike and rake. After eight iterations, only the noisy observation

is showing a significant misfit. Due to the misfit of the noisy observation, the error function vector has a large projection onto the u_3 data eigenvector, which is associated with the smallest single value. The weighting factor a_3 is therefore large (see equation 2). The large factor a_3 is weighting the third model eigenvector v_3, which has components in the strike and rake directions, but not in the dip direction. The parameters strike and rake are therefore changing significantly with each iteration, even though the other 17 waveforms are being fit. Thus, the eigenvectors show that one noisy observation is imposing a dominant control on the parameters strike and rake, but is not influencing dip.

In this case, the use of the maximum likelihood inverse or weighted least-squares is necessary. Table V-4 shows the inversion results using different weighting factors for the noisy observation. Note that for smaller weighting factors, the values of strike, dip, and rake approach the results of the noiseless case (θ = 82°, δ = 68°, λ = 89°) described in the previous section.

Discussion

This inversion method is not limited to data from teleseismic and regional distances alone. As long as the appropriate Green's functions can be generated, body waves for all distances can be inverted for source parameters. For example, if the upper mantle structure is known, then waveforms recorded at upper mantle distances can be added to a data set to provide better coverage and constraints. We have shown that the addition of regional distance waveforms to the data set containing teleseismic information, alone, provides valuable constraints on the source parameter estimates. The robustness of the regional distance Green's functions makes the regional information valuable for constraining source parameter estimates, particularly when the Green's functions for the teleseismic portion of the data set are inadequate. The use of singular value decomposition for the inversion is also particularly useful since it allows direct insight into which observations are providing the greatest influence on the model parameter estimates.

TABLE V-4

INVERSION RESULTS USING MAXIMUM LIKELIHOOD INVERSE

Wt. Factor	Strike	Dip	Rake
.70	92.8	69.5	-103.5
.40	91.3	69.3	-102.0
.10	88.6	69.7	-98.0
.05	86.2	69.0	-95.0
.01	82.0	68.0	-89.2

This method should also prove useful for the inversion of historical data where instrument gain and absolute amplitude are poorly determined and teleseismic station coverage is sparse.

REFERENCES

Aki, K. and Y. B. Tsai (1972). Mechanism of Love wave excitation by explosion sources, J. Geophys. Res. 77, 1452-1475.

Alexander, S. S. (1980). Comparison of source and propagation characteristics in Eurasia, North Africa and the U.S. using regional seismic and remote sensing observations, DARPA Symposium, Grand Island, New York.

Archambeau, C. (1972). The theory of stress wave radiation from explosions in prestressed media, Geophys J. 29 329-366.

Barker, J. S. , L. J. Burdick and T. C. Wallace (1985). Analysis of near-field seismic waveforms from underground nuclear explosions, Scientific Report No. 1, AFGL-TR-85-0321, Woodward Clyde Consultants, Pasadena. ADA165227

Douglas, A., J. B. Young, and N. S. Layman (1985). Spalling and tectonic release associated with underground explosions at the Nevada Test Site: evidence from broad band P waves, Bull. Seism. Soc. Am. 76, 305-311.

Given, J. W. and G. R. Mellman (1985). Source parameters for nuclear explosions at NTS and Shagan River from observations of Rayleigh and Love waves, presented at the DARPA/AFGL Seismic Research Symposium, May 6-8, 1985.

Grand, S. P. and D. V. Helmberger (1984). Upper mantle shear structure of North America, Geophys. J. R. Astr. Soc. 76, 399-438.

Gupta, I. N. and R. R. Blandford (1983). A mechanism for generation of short-period transverse motion from explosions, Bull. Seism. Soc. Am. 73, 933-947.

Helmberger, D. V., G. R. Engen, and S. P. Grand (1985). Upper mantle cross section from California to Greenland, Geophys. J. (in press).

Langston, C. A. and D. V. Helmberger (1975), A procedure for modeling shallow dislocation sources, Geophys. J. R. Astr. Soc. 42, 117-130.

Lay, T., T. C. Wallace, and D. V. Helmberger (1984). The effects of tectonic release on short-period P waves from NTS explosions, Bull. Seism. Soc. Am. 74, 819-842.

Liu, and H. Kanamori (1980). Determination of source parameters of mid-plate earthquakes from the waveforms of body waves, Bull. Seism. Soc. Am. 70, 593-613.

Lynne, C. and T. Lay (1984). Defocussing of short period P waves by a high velocity anomaly beneath Pahute Mesa, EOS, Trans. Am. Geophys. Union 65, 994.

McKeown, F. A. and D. D. Dickey (1969). Fault displacement and motion related to nuclear explosions, Bull. Seism. Soc. Am. 59, 2259-2269.

Pomeroy, P. W., W. J. Best and T. V. McEvilly (1982). Test Ban Treaty verification with regional data--a review, Bull. Seism. Soc. Am. 72, S89-S130.

Stevens, J. L., W. L. Rodi, J. Wang, B. Shkoller, E. J. Halda, B. F. Mason, and J. B. Minster (1982). Surface wave analysis package and Shagan River to SRO station path corrections, S-Cubed Topical Report VSC-TR-82-81.

Wallace, T. C. (1986). Some useful approximations to generalized ray theory for regional distance seismograms, Geophys. J. R. Astr. Soc. 85, 349-363.

Wallace, T. C., D. V. Helmberger, and G. K. Engen (1985). Evidence of tectonic release from underground nuclear explosions in long-period S waves, Bull. Seism. Soc. Am. 85, 157-174.

Wallace, T. C., D. V. Helmberger, and G. K. Engen (1983). Evidence of tectonic release from underground nuclear explosions in long-period P-waves, Bull. Seism. Soc. Am. 73, 593-613.

Wallace, T. C., D. V. Helmberger, and T. Lay (1986). Reply to comments by A. Douglas , J. B. Young and N. S. Lyman and a note on the revised moments for Pahute Mesa tectonic release, Bull. Seism. Soc. Am. 76, 313-318.

Wallace, T. C., D. V. Helmberger, and G. R. Mellman (1981). A technique for the inversion of regional data in source parameter studies, J. Geophys. Res. 86, 1679-1685.

DISTRIBUTION LIST

Dr. Monem Abdel-Gawad
Rockwell Internat'l Science Center
1049 Camino Dos Rios
Thousand Oaks, CA 91360

Professor Keiiti Aki
Center for Earth Sciences
University of Southern California
University Park
Los Angeles, CA 90089-0741

Dr. Raplh Alewine III
DARPA/STO/GSD
1400 Wilson Boulevard
Arlington, CA 22209-2308

Professor Shelton S. Alexander
Geosciences Department
403 Deike Building
The Pennsylvania State University
University Park, PA 16802

Professor Charles B. Archambeau
Cooperative Institute for Resch
in Environmental Sciences
University of Colorado
Boulder, CO 80309

Dr. Thomas C. Bache Jr.
Science Applications Int'l Corp.
10210 Campus Point Drive
San Diego, CA 92121

Dr. Robert Blandford
DARPA/STO/GSD
1400 Wilson Boulevard
Arlington, CA 22209-2308

Dr. Lawrence Braile
Department of Geosciences
Purdue University
West Lafayette, IN 47907

Dr. James Bulau
Rockwell Int'l Science Center
1049 Camino Dos Rios
P.O. Box 1085
Thousand Oaks, CA 91360

Dr. Douglas R. Baumgardt
Signal Analysis & Systems Div.
ENSCO, Inc.
5400 Port Royal Road
Springfield, VA 22151-2388

Dr. G. Blake
US Dept of Energy/DP 331
Forrestal Building
1000 Independence Ave.
Washington, D.C. 20585

Dr. S. Bratt
Science Applications Int'l Corp.
10210 Campus Point Drive
San Diego, CA 92121

Woodward-Clyde Consultants
ATTN: Dr. Lawrence J. Burdick
Dr. Jeff Barker
P.O. Box 93245
Pasadena, CA 91109-3245 (2 copies)

Dr. Roy Burger
1221 Serry Rd.
Schenectady, NY 12309

Professor Robert W. Clayton
Seismological Laboratory/Div. of
Geological & Planetary Sciences
California Institute of Technology
Pasadena, CA 91125

Dr. Vernon F. Cormier/Earth Resources
Lab, Dept of Earth, Atmospheric and
Planetary Sciences
MIT - 42 Carleton Street
Cambridge, MA 02142

Professor Anton W. Dainty
AFGL/LWH
Hanscom AFB, MA 01731

Dr. Zoltan A. Der
ENSCO, Inc.
5400 Port Royal Road
Springfield, VA 22151-2388

Professor Adam Dziewonski
Hoffman Laboratory
Harvard University
20 Oxford St.
Cambridge, MA 02138

Professor John Ebel
Dept of Geology & Geophysics
Boston College
Chestnut Hill, MA 02167

Dr. Jack Evernden
USGS-Earthquake Studies
345 Middlefield Road
Menlo Park, CA 94025

Professor John Ferguson
Center for Lithospheric Studies
The University of Texas at Dallas
P.O. Box 830688
Richardson, TX 75083-0688

Mr. Edward Giller
Pacific Seirra Research Corp.
1401 Wilson Boulevard
Arlington, VA 22209

Dr. Jeffrey W. Given
Sierra Geophysics
11255 Kirkland Way
Kirkland, WA 98033

Professor Steven Grand
Department of Geology
245 Natural History Building
1301 West Green Street
Urbana, IL 61801

Professor Roy Greenfield
Geosciences Department
403 Deike Building
The Pennsylvania State University
University Park, PA 16802

Dr. James Hannon
Lawrence Livermore Nat'l Lab.
P.O. Box 808
Livermore, CA 94550

Professor David G. Harkrider
Seismological Laboratory
Div of Geological & Planetary Sciences
California Institute of Technology
Pasadena, CA 91125

Professor Donald V. Helmberger
Seismological Laboratory
Div of Geological & Planetary Sciences
California Institute of Technology
Pasadena, CA 91125

Professor Eugene Herrin
Institute for the Study of Earth
& Man/Geophysical Laboratory
Southern Methodist University
Dallas, TX 75275

Professor Robert B. Herrmann
Department of Earth & Atmospheric
Sciences
Saint Louis University
Saint Louis, MO 63156

U.S. Arms Control & Disarm. Agency
ATTN: Mrs. M. Hoinkes
Div. of Multilateral Affairs
Room 5499
Washington, D.C. 20451

Professor Lane R. Johnson
Seismographic Station
University of California
Berkeley, CA 94720

Professor Thomas H. Jordan
Department of Earth, Atmospheric
and Planetary Sciences
Mass Institute of Technology
Cambridge, MA 02139

Dr. Alan Kafka
Department of Geology &
Geophysics
Boston College
Chestnut Hill, MA 02167

Ms. Ann Kerr
DARPA/STO/GSD
1400 Wilson Boulevard
Arlington, VA 22209-2308

Professor Charles A. Langston
Geosciences Department
403 Deike Building
The Pennsylvania State University
University Park, PA 16802

Professor Thorne Lay
Department of Geological Sciences
1006 C.C. Little Building
University of Michigan
Ann Harbor, MI 48109-1063

Dr. Arthur Lerner-Lam
Lamont-Doherty Geological Observatory
of Columbia University
Palisades, NY 10964

Dr. George R. Mellman
Sierra Geophysics
11255 Kirkland Way
Kirkland, WA 98033

Professor Brian J. Mitchell
Department of Earth & Atmospheric
Sciences
Saint Louis University
Saint Louis, MO 63156

Professor Thomas V. McEvilly
Seismographic Station
University of California
Berkeley, CA 94720

Dr. Keith L. McLaughlin
Teledyne Geotech
314 Montgomery Street
Alexandria, VA 22314

Mr. Jack Murphy - S-CUBED
Reston Geophysics Office
11800 Sunrise Valley Drive
Suite 1212
Reston, VA 22091

Dr. Carl Newton
Los Alamos National Lab.
P.O. Box 1663
Mail Stop C335, Group E553
Los Alamos, NM 87545

Professor Otto W. Nuttli
Department of Earth &
Atmospheric Sciences
Saint Louis University
Saint Louis, MO 63156

Professor J. A. Orcutt
Geological Sciences Div.
Univ. of California at
San Diego
La Jolla, CA 92093

Dr. Frank F. Pilotte
Director of Geophysics
Headquarters Air Force Technical
Applications Center
Patrick AFB, Florida 32925-6001

Professor Keith Priestley
University of Nevada
Mackay School of Mines
Reno, Nevada 89557

Mr. Jack Raclin
USGS - Geology, Rm 3 C136
Mail Stop 928 National Center
Reston, VA 22092

Professor Paul G. Richards
Lamont-Doherty Geological
Observatory of Columbia Univ.
Palisades, NY 10964

Dr. Norton Rimer
S-CUBED
A Division of Maxwell Lab
P.O. 1620
La Jolla, CA 92038-1620

Dr. George H. Rothe
Chief, Research Division
Geophysics Directorate
HQ Air Force Technical
Applications Center
Patrick AFB, Florida 32925-6001

Professor Larry J. Ruff
Department of Geological Sciences
1006 C.C. Little Building
University of Michigan
Ann Arbor, MI 48109-1063

Dr. Alan S. Ryall, Jr.
Center of Seismic Studies
1300 North 17th Street
Suite 1450
Arlington, VA 22209-2308

Professor Charles G. Sammis
Center for Earth Sciences
University of Southern California
University Park
Los Angeles, CA 90089-0741

Dr. David G. Simpson
Lamont-Doherty Geological Observ.
of Columbia University
Palisades, NY 10964

Dr. Jeffrey L. Stevens
S-CUBED,
A Division of Maxwell Laboratory
P.O. Box 1620
La Jolla, CA 92038-1620

Professor Brian Stump
Institute for the Study of Earth & Man
Geophysical Laboratory
Southern Methodist University
Dallas, TX 75275

Professor Ta-liang Teng
Center for Earth Sciences
University of Southern California
University Park
Los Angeles, CA 90089-0741

Dr. R. B. Tittmann
Rockwell International Science Ctr
1049 Camino Dos Rios
P.O. Box 1085
Thousand Oaks, CA 91360

Professor M. Nafi Toksoz/Earth Resources
Lab - Dept of Earth, Atmospheric and
Planetary Sciences
MIT - 42 Carleton Street
Cambridge, MA 02142

Dr. Lawrence Turnbull
OSWR/NED
Central Intelligence Agency
CIA, Room 5G48
Washington, D.C. 20505

Professor Terry C. Wallace
Department of Geosciences
Building #11
University of Arizona
Tucson, AZ 85721

Professor John H. Woodhouse
Hoffman Laboratory
Harvard University
20 Oxford St.
Cambridge, MA 02138

***

DARPA/PM
1400 Wilson Boulevard
Arlington, VA 22209

Defense Technical
Information Center
Cameron Station
Alexandria, VA 22314
(12 copies)

Defense Intelligence Agency
Directorate for Scientific &
Technical Intelligence
Washington, D.C. 20301

Defense Nuclear Agency/SPSS
ATTN: Dr. Michael Shore
6801 Telegraph Road
Alexandria, VA 22310

AFOSR/NPG
ATTN: Director
Bldg 410, Room C222
Bolling AFB, Wash D.C. 20332

AFTAC/CA (STINFO)
Patrick AFB, FL 32925-6001

U.S. Geological Survey
ATTN: Dr. T. Hanks
Nat'l Earthquake Resch Center
345 Middlefield Road
Menlo Park, CA 94025

SRI International
333 Ravensworth Avenue
Menlo Park, CA 94025

Center for Seismic Studies
ATTN: Dr. C. Romney
1300 North 17th St., Suite 1450
Arlington, VA 22209 (3 copies)

Science Horizons, Inc.
ATTN: Dr. Bernard Minster
Dr. Theodore Cherry
710 Encinitas Blvd., Suite 101
Encinitas, CA 92024 (2 copies)

Dr. G. A. Bollinger
Department of Geological Sciences
Virginia Polytechnical Institute
21044 Derring Hall
Blacksburg, VA 24061

Dr. L. Sykes
Lamont Doherty Geological Observ.
Columbia University
Palisades, NY 10964

Dr. S. W. Smith
Geophysics Program
University of Washington
Seattle, WA 98195

Dr. L. Timothy Long
School of Geophysical Sciences
Georgia Institute of Technology
Atlanta, GA 30332

Dr. N. Biswas
Geophysical Institute
University of Alaska
Fairbanks, AK 99701

Dr. Freeman Gilbert - Institute of
Geophysics & Planetary Physics
Univ. of California at San Diego
P.O. Box 109
La Jolla, CA 92037

Dr. Pradeep Talwani
Department of Geological Sciences
University of South Carolina
Columbia, SC 29208

Dr. Donald Forsyth
Dept. of Geological Sciences
Brown University
Providence, RI 02912

Dr. Jack Oliver
Department of Geology
Cornell University
Ithaca, NY 14850

Dr. Muawia Barazangi
Geological Sciences
Cornell University
Ithaca, NY 14853

Rondout Associates
ATTN: Dr. George Sutton,
Dr. Jerry Carter, Dr. Paul Pomeroy
P.O. Box 224
Stone Ridge, NY 12484 (3 copies)

Dr. Bob Smith
Department of Geophysics
University of Utah
1400 East 2nd South
Salt Lake City, UT 84112

Dr. Anthony Gangi
Texas A&M University
Department of Geophysics
College Station, TX 77843

Dr. Gregory B. Young
ENSCO, Inc.
5400 Port Royal Road
Springfield, CA 22151

Weidlinger Associates
ATTN: Dr. Gregory Wojcik
620 Hansen Way, Suite 100
Palo Alto, CA 94304

Dr. Leon Knopoff
University of California
Institute of Geophysics
& Planetary Physics
Los Angeles, CA 90024

Dr. Kenneth H. Olsen
Los Alamos Scientific Lab.
Post Office Box 1663
Los Alamos, NM 87545

Professor Jon F. Claerbout
Professor Amos Nur
Dept. of Geophysics
Stanford University
Stanford, CA 94305 (2 copies)

Dr. Robert Burridge
Schlumberger-Doll Resch Ctr.
Old Quarry Road
Ridgefield, CT 06877

Dr. Robert Phinney/Dr. F.A. Dahlen
Dept of Geological
Geophysical Sci. University
Princeton University
Princeton, NJ 08540 (2 copies)

New England Research, Inc.
ATTN: Dr. Randolph Martin III
P.O. Box 857
Norwich, VT 05055

Sandia National Laboratory
ATTN: Dr. H. B. Durham
Albuquerque, NM 87185

AFGL/XO
Hanscom AFB, MA 01731-5000

AFGL/LW
Hanscom AFB, MA 01731-5000

AFGL/SULL
Research Library
Hanscom AFB, MA 01731-5000 (2 copies)

Secretary of the Air Force (SAFRD)
Washington, DC 20330

Office of the Secretary Defense
DDR & E
Washington, DC 20330

HQ DNA
ATTN: Technical Library
Washington, DC 20305

Director, Technical Information
DARPA
1400 Wilson Blvd.
Arlington, VA 22209

Los Alamos Scientific Laboratory
ATTN: Report Library
Post Office Box 1663
Los Alamos, NM 87544

Dr. Thomas Weaver
Los Alamos Scientific Laboratory
Los Almos, NM 97544

Dr. Gary McCartor
Mission Research Corp.
735 State Street
P.O. Drawer 719
Santa Barbara, CA 93102

Dr. Al Florence
SRI International
333 Ravenwood Avenue
Menlo Park, CA 94025-3493

Dr. W. H. K. Lee
USGS
Office of Earthquakes, Volcanoes,
& Engineering
Branch of Seismology
345 Middlefield Rd
Menlo Park, CA 94025

***

Dr. Peter Basham/Earth Physics Branch
Department of Energy and Mines
1 Observatory Crescent
Ottawa, Ontario
CANADA K1A 0Y3

Dr. Eduard Berg
Institute of Geophysics
University of Hawaii
Honolulu, HI 96822

Dr. Michel Bouchon - Universite
Scientifique et Medicale de Grenob
Lab de Geophysique - Interne et
Tectonophysique - I.R.I.G.M-B.P.
38402 St. Martin D'Heres
Cedex FRANCE

Dr. Hilmar Bungum/NTNF/NORSAR
P.O. Box 51
Norwegian Council of Science,
Industry and Research, NORSAR
N-2007 Kjeller, NORWAY

Dr. Kin-Yip Chun
Geophysics Division
Physics Department
University of Toronto
Ontario, CANADA M5S 1A7

Dr. Alan Douglas
Ministry of Defense
Blacknest, Brimpton,
Reading RG7-4RS
UNITED KINGDOM

Professor Peter Harjes
Institute for Geophysik
Rhur University/Bochum
P.O. Box 102148, 4630 Bochum 1
FEDERAL REPUBLIC OF GERMANY

Dr. E. Husebye
NTNF/NORSAR
P.O. Box 51
N-2007 Kjeller, NORWAY

Mr. Peter Marshall, Procurement
Executive, Ministry of Defense
Blacknest, Brimpton,
Reading FG7-4RS
UNITED KINGDOM

Dr. B. Massinon
Societe Radiomana
27, Rue Claude Bernard
75005, Paris, FRANCE

Dr. Pierre Mechler
Societe Radiomana
27, Rue Claude Bernard
75005, Paris, FRANCE

Dr. Ben Menaheim
Weizman Institute of Science
Rehovot, ISRAEL 951729

Dr. Svein Mykkeltveit
NTNF/NORSAR
P.O. Box 51
N-2007 Kjeller, NORWAY

Dr. Frode Ringdal
NTNF/NORSAR
P.O. Box 51
N-2007 Kjeller, NORWAY

University of Hawaii
Institute of Geophysics
ATTN: Dr. Daniel Walker
Honolulu, HI 96822

***

END

DATE

FILMED

8-88

DTIC